Theoretical studies of unconventional superconductors

Martin Sigurd Grønsleth

Thesis for the degree philosophiæ doctor

March 2008

NTNU
Norwegian University of
Science and Technology

Faculty of Natural Science and Technology
Department of Physics
NTNU Trondheim

Abstract

This thesis presents four research papers. In the first three papers we have derived analytical results for the transport properties in unconventional superconductors and ferromagnetic systems with multiple broken symmetries. In Paper I and parts of Paper II we have studied tunneling transport between two non-unitary ferromagnetic spin-triplet superconductors, and found a novel interplay between ferromagnetism and superconductivity manifested in the Josephson effect as a spin- and charge-current in the absence of an applied voltage across the junction. The critical amplitudes of these currents can be adjusted by the relative magnetization direction on each side of the junction. Furthermore, in Paper II, we have found a way of controlling a spin-current between two ferromagnets with spin-orbit coupling. Paper III considers a junction consisting of a ferromagnet and a non-unitary ferromagnetic superconductor, and we show that the conductance spectra contains detailed information about the superconducting gaps and pairing symmetry of the Cooper-pairs.

In the last paper we present a Monte Carlo study of an effective Hamiltonian describing orbital currents in the CuO_2 layers of high-temperature superconductive cuprates. The model features two intrinsically anisotropic Ising models, coupled through an anisotropic next-nearest neighbor interaction, and an Ashkin–Teller nearest neighbor fourth order coupling. We have studied the specific heat anomaly, as well as the anomaly in the staggered magnetization associated with the orbital currents and its susceptibility. We have found that in a limited parameter regime, the specific heat anomaly is substantially suppressed, while the susceptibility has a non-analytical peak across the order-disorder transition. The model is therefore a candidate for describing the breakup of hidden order when crossing the pseudo-gap line on the under-doped side in the phase diagram of high-temperature superconductors.

Preface

This thesis is submitted as part of the requirement for the degree Philosophiae Doctor at the Norwegian University of Science and Technology (NTNU). The study has been performed at the Department of Physics, where my supervisor has been Professor Asle Sudbø, to whom I am very grateful for giving me the opportunity to work with these interesting and challenging subjects.

My work started in August 2003 and ended April 2008. That also includes teaching duties equivalent to one year, as well as courses amounting to one full semester. The study was funded by the Research Council of Norway through a project in the NANOMAT program with the title "Nationally Coordinated Project in Oxides for Future Information and Communication Technology".

Parts of the work were done in collaboration with Jon-Mattis Børven, Eskil Kulseth Dahl, Jacob Linder and Trond Bergh Nilssen who also are (co-)authors of the papers presented in this thesis. The Monte Carlo code I have used is based on a library developed by Joakim Hove, and the simulations have been performed at the supercomputing facilities at NTNU (using `gridur`, `embla` and `njord`) and at the University of Tromsø (using `stallo`). In addition to those already mentioned, I very much acknowledge Prof. Chandra Varma for co-authoring the last paper.

During my study, I have attended several conferences, most notably the APS March meeting in 2006 where I held a talk and presented some of my work. In April and May 2007 I was located at the Centre for Advanced Study in Oslo.

In the first part of this thesis a brief introduction to the field of research and motivation for the work is given. In the second part the main results of our research is presented in the four papers that I have taken part in during my PhD study.

Martin S. Grønsleth
Trondheim, March 2008

List of papers

Paper I

M. S. Grønsleth, J. Linder, J.-M. Børven, and A. Sudbø

Interplay between Ferromagnetism and Superconductivity in Tunneling Currents

Physical Review Letters, **97**, 147002 (2006) [1] `arXiv:cond-mat/0412193`

We study tunneling currents in a model consisting of two non-unitary ferromagnetic spin-triplet superconductors separated by a thin insulating layer. We find a novel interplay between ferromagnetism and superconductivity, manifested in the Josephson effect. This offers the possibility of tuning dissipationless currents of charge and spin in a well-defined manner by adjusting the magnetization direction on either side of the junction.

Paper II

J. Linder, M. S. Grønsleth, and A. Sudbø

Tunneling currents in ferromagnetic systems with multiple broken symmetries

Physical Review B, **75**, 024508 (2007) [2] `arXiv:cond-mat/0609314`

A system exhibiting multiple simultaneously broken symmetries offers the opportunity to influence physical phenomena such as tunneling currents by means of external control parameters. In this paper, we consider the broken $SU(2)$ (internal spin) symmetry of ferromagnetic systems coexisting with *(i)* the broken $U(1)$ symmetry of superconductors and *(ii)* the broken spatial inversion symmetry induced by a Rashba term in a spin-orbit coupling Hamiltonian. In order to study the effect of these broken symmetries, we consider tunneling currents that arise in two different systems; tunneling junctions consisting of non-unitary spin-triplet ferromagnetic superconductors and junctions consisting of ferromagnets with spin-orbit coupling. In the former case, we consider different pairing symmetries in a model where ferromagnetism and superconductivity coexist uniformly. An interplay between the relative magnetization orientation on each side of the junction and the superconducting phase difference

is found, similar to that found in earlier studies on spin-singlet superconductivity coexisting with spiral magnetism. This interplay gives rise to persistent spin- and charge-currents in the absence of an electrostatic voltage that can be controlled by adjusting the relative magnetization orientation on each side of the junction. In the second system, we study transport of spin in a system consisting of two ferromagnets with spin-orbit coupling separated by an insulating tunneling junction. A persistent spin-current across the junction is found, which can be controlled in a well-defined manner by external magnetic and electric fields. The behavior of this spin-current for important geometries and limits is studied.

Paper III

J. Linder, M. S. Grønsleth, and A. Sudbø

Conductance spectra of ferromagnetic superconductors: Quantum transport in a ferromagnetic metal/non-unitary ferromagnetic superconductor junction

Physical Review B, **75**, 054518 (2007) [3] `arXiv:cond-mat/0611242`

Recent findings of superconductors that simultaneously exhibit multiple spontaneously broken symmetries, such as ferromagnetic order or lack of an inversion center and even combinations of such broken symmetries, have led to much theoretical and experimental research. We consider quantum transport in a junction consisting of a ferromagnetic metal and a non-unitary ferromagnetic superconductor. It is shown that the conductance spectra provide detailed information about the superconducting gaps, and are thus helpful in determining the pairing symmetry of the Cooper-pairs in ferromagnetic superconductors.

Paper IV

M. S. Grønsleth, T. B. Nilssen, E. K. Dahl, C. M. Varma, and A. Sudbø

Specific heat, order parameter, and magnetic susceptibility from fluctuating orbital currents in high-T_c superconducting cuprates

Preprint

We have performed large-scale Monte Carlo simulations on a two-dimensional generalized Ising model of thermally fluctuating orbital currents in CuO_2-plaquettes of high-T_c cuprates. The Ising variables represent Cu-Cu bond-currents on the lattice. The model features intrinsically anisotropic Ising couplings, as well as an anisotropic next-nearest neighbor interaction which tends to frustrate uniform ordering in the system. In addition, the model features an Ashkin–Teller nearest-neighbor four-spin

coupling. We find that the specific heat features a substantially suppressed anomaly compared to the logarithmic singularity of the 2D Ising model. The anomaly does not appear to scale with system size for finite antiferromagnetic Ashkin–Teller coupling. We also compute the staggered magnetization of the system associated with ordering of the orbital currents. We find that the staggered magnetization as well as its susceptibility has the same characteristics as for the 2D Ising model with a pronounced and easily discernible non-analytic behavior across the order-disorder transition. The non-analytic behavior of the staggered magnetization implies that a field-induced *uniform* magnetization also will feature non-analyticities across the phase transition. A prediction from our calculations is therefore that a uniform field-induced magnetization M_0 should have a non-analytic behavior across the pseudogap line of high-T_c cuprates on the underdoped side, as the staggered orbital magnetic moment originating with the orbital currents within each unit cell sets in. Specifically, we predict that M_0 induced by a magnetic field H perpendicular to the CuO_2-plane will have the form $H/M_0 = A + B\ \Theta(T_c - T)\ |1 - T/T_c|^{2\beta}$, where Θ is a step-function, and β is a non-universal order-parameter exponent of the *staggered* magnetization with a value $1/8 < \beta < 1/4$.

My contribution to the papers

In Paper I and II [1, 2] I have contributed substantially to all parts of the papers. I have performed the majority of the calculations and contributed to all parts of the text.

In Paper III [3] I have contributed to the model formulation and in analyzing the results. Moreover, I took part in writing the paper.

In Paper IV [4] I wrote some of the key parts of the code, performed a substantial part of the Monte Carlo simulations, developed scripts for post-processing the data and for generating plots. I also took part in interpreting the results, and was involved in writing the paper.

Table of Contents

List of Figures

1 Introduction

Some everyday tools, such as a *compass*, are based on the discovery of simple physical principles that reveal themselves in a straight forward way. In the case of the compass, it was found that a magnetized needle placed in a cork floating in a bowl of water would have one end pointing towards the (magnetic) north pole. Without further understanding of the underlying physical concept of *magnetism*, this device proved extremely useful for giving directions at sea since some thousand years back.

Today, the fundamental physics behind magnetism is much better understood, due to both theoretical and experimental scientific research. Consequently, this has led to much more sophisticated technology, such as devices for storing information on rotating disks coated in a magnetic material, more commonly known as *hard disk drives*.

Superconductivity is another "everyday phenomenon", at least in terms of its wide use in for example medical imaging. Although one group of superconductors, the so-called *conventional superconductors*, are well understood even at the microscopic level, there are many open questions about how *high-temperature superconductors* really function. Nevertheless, we are able to make use of their physical *properties*, without knowing how they really come about. The aim is, however, to get to know the fundamental underlying physics on the microscopic scale, and thereby learn how to tweak these materials to, for example, become superconducting even at room-temperature. The potential for industrial applications is enormous.

The ancient idea that everything in this world consists of *earth, water, air* and/or *fire*, was rejected long ago. The more modern categorization into *solid, liquid* or *gas* states works well in the kitchen, but is far from sufficient at describing the radically different properties of a normal conductor and a superconductor, or even distinguishing a magnetic metal from a non-magnetic one. The concept of *broken symmetries*, however, is a neat way of classifying matter. In this scheme, we classify states of matter (primarily) by what *symmetries* are "broken" and what the *order parameters* are. In the case of the magnet

in its magnetized state, the order parameter is the *magnetization vector*, which points in a given direction in space, and the lost symmetry is the rotational invariance, denoted $SO(3)$.[1] More details on this is left for later treatment in this thesis—the point to be made here is that this scheme serves as a structured and very powerful way of treating physical systems theoretically. This will be prominent in this thesis.

Many physical concepts are well understood in their pure form, in which they have been studied as isolated properties. *Tunneling transport* between two conventional superconductors is one example. A conventional superconductor in its superconducting phase possess what we call a broken $U(1)$-symmetry, where the state has acquired a given phase. Now, if we introduce a *new* broken symmetry to such a system, for example magnetization, characterized by the loss of $SO(3)$-symmetry as mentioned above, we expect new transport properties to unfold. Specifically, we would expect the internal magnetic moment of the electrons to enter the equations. Much of this thesis is concerned with systems that are characterized by two or more broken symmetries.

Outline

Apart from the papers, this thesis consists of three main introductory parts. In Chapter 2, a brief introduction to some general concepts is given. It serves as a theoretical base for what follows, and does not include any motivation for the work. This chapter can be skipped by the experienced reader. In Chapter 3 more specific formalism and theory is introduced which form the basis for the papers. Chapter 4 (Paper I-III [1, 2, 3]) and 5 (Paper IV [4]) present the motivation for the work and touch upon the results of the papers. Acknowledgments can be found in the last chapter.

[1] Okay, the symmetry is of course not entirely *broken*—in this case it is rather *reduced*. It is sometimes more precise to say that the *state* is *fixed*.

2 General concepts

This chapter will provide a brief summary of some mathematical tools and physical concepts that are important for the subsequent discussion. It also serves as an introduction to the notation used in the papers.

It is not meant as a comprehensive theoretical introduction, but rather to serve as a quick reminder for readers who are already familiar with the field. Some sections, however, include some basic notions that are meant for the novice reader. Natural units are used where suitable.

2.1 Second quantization

In the field of condensed matter physics one is typically interested in calculating physical observables from a microscopic description of a system. The microscopic model is usually defined by the *Hamiltonian*, or in the first quantization formulation, the Hamilton operator. It can often be described by three terms,

$$\begin{aligned} \hat{H}_{\text{Total}} &= \hat{T} + \hat{U} + \hat{V} \\ &= \sum_i \frac{\hat{\boldsymbol{p}}_i^2}{2m} + \sum_i U(\boldsymbol{r}_i) + \sum_{i<j} V(\boldsymbol{r}_i, \boldsymbol{r}_j), \end{aligned} \tag{2.1}$$

where the first term $\hat{T}$ describes the kinetic energy of the particles, m is the particle mass, and $\hat{\boldsymbol{p}} = -\mathrm{i}\hbar\nabla$ is the momentum operator. For simplicity we have here assumed that the external potential U and the particle-particle interaction V are independent of any internal degrees of freedom, such as the electron spin. The sums are over all N particles in the system, in the last term only for indices $i < j$ to avoid double counting.

It is the interaction term that makes the Hamiltonian hard to solve—if the last term was zero, the solution would simply be the sum of the individual single particle solutions.

If we let $\Psi(\boldsymbol{r}_1, \boldsymbol{r}_2, \ldots, \boldsymbol{r}_N)$ denote the many-particle wave function that holds all relevant information about the system, we can (in principle) solve the Schrödinger equation

$$\hat{H}\Psi(\boldsymbol{r}_1, \boldsymbol{r}_2, \ldots, \boldsymbol{r}_N) = E\Psi(\boldsymbol{r}_1, \boldsymbol{r}_2, \ldots, \boldsymbol{r}_N), \tag{2.2}$$

if we assume a stationary state. Together with a set of boundary conditions[1] appropriate for the system in question, this eigenvalue equation will reveal all valid energy levels E of the system.

It turns out, however, that when we deal with many-particle systems with identical particles, such as condensed matter systems where we want to describe the electrons, Eq. (2.2) usually becomes incomprehensible. We will therefore turn to the *second quantized* formulation.

Creation and annihilation

The discussion here will be confined to a quick summary of some key properties of the creation and annihilation operators for fermions. For a more complete introduction to second quantization[2], the books by Gross, Runge and Heinonen [5] as well as Mandl and Shaw [6] can be recommended.

The state Ψ of an interacting many-particle system is in the second quantized version expressed in terms of occupation numbers,

$$\begin{aligned} |\Psi\rangle &= |\ldots, n_{\lambda_{i-1}}, n_{\lambda_i}, n_{\lambda_{i+1}}, \ldots\rangle \\ &= \prod_i |n_{\lambda_i}\rangle, \end{aligned} \tag{2.3}$$

where λ_i is a set of quantum numbers for particle i, for example for the spin projection $\sigma \in \pm 1$ we would have $\lambda = (\boldsymbol{k}, \sigma)$ for fermions with momentum $\boldsymbol{k}$, or $\lambda = (\boldsymbol{r}, \sigma)$ in real space position $\boldsymbol{r}$. The occupation number n_λ denotes how many particles that are in the given state. For fermions, only one particle can occupy each state, which is known as the *Pauli exclusion principle*. Therefore, $n_\lambda \in \{0, 1\}$, *i.e.* a state is either occupied or unoccupied.

The creation operator $c_\lambda^\dagger$ and the annihilation operator c_λ can alter the state $|\Psi\rangle$ according to

$$c_\lambda^\dagger|\Psi\rangle = (-1)^{[\sum_{\lambda'<\lambda} n_{\lambda'}]}\sqrt{1-n_\lambda}|\ldots, (n_\lambda+1), \ldots\rangle, \tag{2.4a}$$

$$c_\lambda|\Psi\rangle = (-1)^{[\sum_{\lambda'<\lambda} n_{\lambda'}]}\sqrt{n_\lambda}|\ldots, (n_\lambda-1), \ldots\rangle. \tag{2.4b}$$

[1] It is these boundary conditions that leads to *quantization*, *i.e.* discrete energy levels etc.

[2] *Second quantization* is often referred to as *canonical quantization*.

It follows that $c_\lambda|0\rangle = 0$, where $|0\rangle$ is the vacuum state, and for example $c^\dagger_{\lambda_i}|0\rangle = |0,\ldots,0,1_{\lambda_i},0,\ldots,0\rangle$. The sign in front in (2.4) is due to the anti-symmetric nature of the fermions, which can be expressed by the anti-commutator relations,

$$\{c_\lambda, c^\dagger_{\lambda'}\} = \delta_{\lambda,\lambda'}, \tag{2.5a}$$

$$\{c_\lambda, c_{\lambda'}\} = 0, \tag{2.5b}$$

$$\{c^\dagger_\lambda, c^\dagger_{\lambda'}\} = 0, \tag{2.5c}$$

where $\{A, B\} \equiv AB + BA$, and $\delta_{\lambda,\lambda'}$ is the Kronecker delta in the quantum numbers λ and λ'.

As an example, the first term $\hat{T}$ in (2.1), which alone describes a free Fermi gas, can be expressed by

$$\hat{T} = \sum_{\langle i,j\rangle,\sigma} \tilde{t}_{ij} c^\dagger_{i\sigma} c_{j\sigma}, \tag{2.6a}$$

where $\langle\cdot,\cdot\rangle$ means that only nearest neighbors should be considered and

$$\tilde{t}_{ij} = \langle\lambda_i|\frac{\hat{\boldsymbol{p}}^2}{2m}|\lambda_j\rangle. \tag{2.6b}$$

The last equation gives a relation between the operator $\hat{\boldsymbol{p}}$ and the second quantized matrix element $\tilde{t}$.

Instead of expressing a given state in terms of the position i, one can use the momentum space representation, given by the (lattice) Fourier transformation of the fermion operators,

$$c_{\boldsymbol{k}\sigma} = \frac{1}{\sqrt{N}} \sum_i c_{i\sigma}\, \mathrm{e}^{-\mathrm{i}\boldsymbol{k}\cdot\boldsymbol{r}_i}, \tag{2.7a}$$

$$c_{i\sigma} = \frac{1}{\sqrt{N}} \sum_{\boldsymbol{k}} c_{\boldsymbol{k}\sigma}\, \mathrm{e}^{\mathrm{i}\boldsymbol{k}\cdot\boldsymbol{r}_i}\,. \tag{2.7b}$$

This can now be inserted in (2.6a) to give $\hat{T} = \sum_{\boldsymbol{k}\sigma} \varepsilon_{\boldsymbol{k}} c^\dagger_{\boldsymbol{k}\sigma} c_{\boldsymbol{k}\sigma}$, where $\varepsilon_{\boldsymbol{k}}$ is the dispersion relation.

One advantage of the second quantized formulation is that it automatically takes care of what is known as the quantum mechanical *principle of indistinguishability of identical particles*. That is, if one for example interchange two electrons of spin up, the wave-function will only acquire a phase. This is what leads to the possible sign in (2.4). This way, one avoids a lot of the redundant information that would otherwise be present in the wave-function. Furthermore, the formulation is convenient for systems where the particle number is not conserved, or where a wave-function formulation doesn't exist.

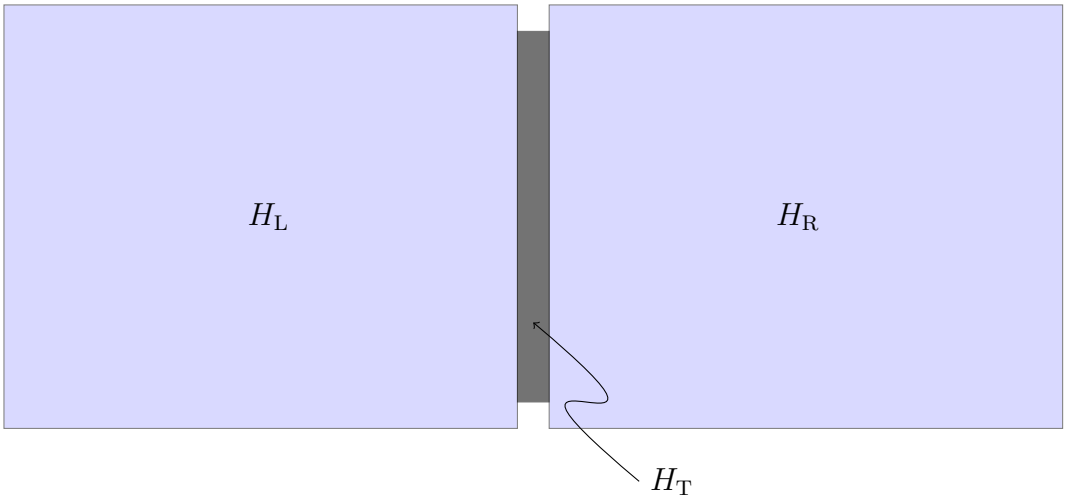

Figure 2.1: Tunneling between two materials through an insulating layer.

2.1.1 Tunneling formalism

The second quantized notation proves to be useful in other contexts as well. For example, if we want to study particle transport between two materials separated by an insulating layer, as shown in Figure 2.1, we can write down the Hamiltonian

$$H = H_{\mathrm{L}} + H_{\mathrm{R}} + H_{\mathrm{T}}. \tag{2.8}$$

Here, H_{L} and H_{R} are the isolated parts of the left and right hand side, respectively, and the tunneling Hamiltonian H_{T} describes the tunneling between the two sides,

$$H_{\mathrm{T}} = \sum_{\boldsymbol{k}\boldsymbol{p}\sigma} \left(T_{\boldsymbol{k}\boldsymbol{p}} c^{\dagger}_{\boldsymbol{k}\sigma} d_{\boldsymbol{p}\sigma} + T^{*}_{\boldsymbol{k}\boldsymbol{p}} d^{\dagger}_{\boldsymbol{p}\sigma} c_{\boldsymbol{k}\sigma} \right). \tag{2.9}$$

In (2.9) the notation is as follows: On the right side the fermion operator is denoted $c_{\boldsymbol{k}\sigma}$ and the momentum is $\boldsymbol{k}$, whereas on the left side we have $d_{\boldsymbol{p}\sigma}$ and $\boldsymbol{p}$. Therefore, the last term in (2.9) annihilates an electron on the right hand side, and creates an electron on the left side, *i.e.* it transfers one electron over the junction. The first term does the opposite.

This formulation was introduced by Cohen in 1962 [7]. Although it might seem as a naive approach, it was utilized by Josephson to correctly predict the two-particle supercurrent that arises in superconducting junctions [8], now known as the Josephson current. More rigorously, it was shown to be correct to the first order in perturbation theory by Prange [9].[3]

[3] Who also acknowledges Josephson's result in a note.

2.2 Green's functions

When describing a condensed matter system, one is often faced with a Hamiltonian of the form

$$H = H_0 + V, \tag{2.10}$$

where H_0 is a part that can be solved exactly, whereas V includes some interactions that makes a direct approach extremely hard to pursue, if not impossible. If H_0 is chosen so that the effect of V is small, one can treat V perturbatively. One starts out by describing the system with H_0 alone, and then introduce V as a small correction, to see how that changes the system. For this approach, the *interaction representation* is most convenient. It is a representation that in some sense is a mix of the Schrödinger representation (where the wave functions are time-dependent and the operators are not) and the Heisenberg representation (where the operators are time-dependent, and the wave functions are not). Specifically, in the interaction picture, the operators and wave functions are given a time-dependence

$$\begin{aligned} \hat{O}(t) &= \mathrm{e}^{\mathrm{i}H_0 t}\, O\, \mathrm{e}^{-\mathrm{i}H_0 t} \\ \hat{\Psi}(t) &= \mathrm{e}^{\mathrm{i}H_0 t}\, \mathrm{e}^{-\mathrm{i}H t}\, \Psi(0), \end{aligned} \tag{2.11}$$

respectively. In order to calculate the response to the perturbation V, we introduce Green's functions.

At zero temperature the single-particle fermion Green function is given by

$$G(\lambda_1, t_1; \lambda_2, t_2) = -\mathrm{i}\langle|\mathrm{T}_t\, c_{\lambda_1}(t_1) c^\dagger_{\lambda_2}(t_2)|\rangle, \tag{2.12}$$

where T_t is time ordering and λ is any quantum number, typically the wave vector $\boldsymbol{k}$ and spin σ, so that $\lambda = (\boldsymbol{k}, \sigma)$. Thus, the Green function represents a *propagator*; for $t_2 < t_1$ it is the probability amplitude for the propagation of an additional particle in state λ_2 at time t_2 to state λ_1 at time t_1. Here, $|\rangle$ represents the ground state, and the operators $c_\lambda(t)$ are represented in the Heisenberg picture, $c_\lambda(t) = \mathrm{e}^{\mathrm{i}(H-\mu N)t}\, c_\lambda\, \mathrm{e}^{-\mathrm{i}(H-\mu N)t}$, where μ is the chemical potential and N is the particle number operator.

2.2.1 Matsubara–Green functions

When we take temperature into account, things get slightly more complicated, because we need to include the statistical operator $\mathrm{e}^{-\beta H}$ in the treatment. Luckily, Matsubara [10] saw the formal similarities between this operator and the quantum mechanical time-evolution operator $\mathrm{e}^{\mathrm{i}Ht}$. As a result, he introduced thermal (temperature-dependent) Green functions which we call the Matsubara–Green functions, where the inverse temperature $\beta = 1/k_\mathrm{B}T$ is treated as a complex time.

The Green function in (2.12) is also valid for non-zero temperatures if we exchange the brackets with the thermodynamical average, which is a trace over the complete set of states $\langle O \rangle = \mathrm{Tr}[\mathrm{e}^{-\beta(H-\mu N-\Omega)}\, O]$, where the thermodynamical potential Ω is given by $\mathrm{e}^{-\beta\Omega} = \mathrm{Tr}[\mathrm{e}^{-\beta(H-\mu N)}]$. The Matsubara–Green function is given by

$$G(\lambda_1, \tau_1; \lambda_2, \tau_2) = -\left\langle \mathrm{T}_\tau\, c_{\lambda_1}(\tau_1) c^\dagger_{\lambda_2}(\tau_2) \right\rangle, \tag{2.13}$$

where $c_\lambda(\tau) = \mathrm{e}^{(H-\mu N)\tau}\, c_\lambda\, \mathrm{e}^{-(H-\mu N)\tau}$. In this notation it is much more convenient to calculate expectation values by means of Matsubara sums over Matsubara frequencies, and then get back to the real time Green functions by analytical continuation. The Matsubara (temperature) Green function can be expressed in frequencies by the Fourier transform

$$G(\lambda, \tau) = \frac{1}{\beta} \sum_{\mathrm{i}\omega_n} \mathrm{e}^{-\mathrm{i}\omega_n \tau}\, \tilde{G}(\lambda, \mathrm{i}\omega_n) \tag{2.14a}$$

$$\tilde{G}(\lambda, \mathrm{i}\omega_n) = \int_0^\beta \mathrm{d}\tau\, \mathrm{e}^{\mathrm{i}\omega_n \tau}\, G(\lambda, \tau), \tag{2.14b}$$

where n is an integer and

$$\omega_n = \begin{cases} \frac{(2n+1)\pi}{\beta} & \text{for fermions.} \\ \frac{2n\pi}{\beta} & \text{for bosons.} \end{cases} \tag{2.15}$$

The formalism is not restricted to single-particle propagators, and is useful in the derivation of spin- and charge-currents when using linear response theory. A comprehensive introduction to Green's functions is given in *e.g.* Refs. [11, 12].

2.2.2 Linear response theory and the Kubo formula

In order to get qualitative results out of the tunneling formalism introduced in Section 2.1.1, one can make use of linear response theory [13, 14]. In short, what one does, is to consider each subsystem in equilibrium, and treat the tunneling part as a small perturbation (that does not give any feedback to the system).

If we let $H(t) = H_0 + H_1(t)$, where H_0 is the unperturbed Hamiltonian and $H_1(t)$ is a small perturbation that we assume is vanishing at $t = -\infty$, we can express the current as

$$\langle J(t) \rangle = -\mathrm{i} \int_{-\infty}^{t} \mathrm{d}t' \, \langle [J(t), H_1(t')] \rangle \,, \tag{2.16}$$

where the left hand side is the real measurable current in the perturbed state, whereas on the right hand side the expectation value is evaluated in the unperturbed state. What Eq. (2.16) expresses, is simply that the output at time t depends not only on the present value, but also on all past values.

2.3 BTK formalism

One weakness of the tunneling formalism given in Section 2.1.1, is that it is only good for high-barrier tunnel junctions, such as insulating oxide layers. For a better treatment of junctions with varying barrier strengths, the so-called *BTK formalism* introduced by Blonder, Tinkham and Klapwijk [15] can be used. The formalism is based on matching of the slope and value of the wave functions across the junction, and considers the probabilities of all possible outcomes of an incident electron. The details will not be presented here, but one important quality of the model is that it accounts for Andreev reflection at the interfaces. For a rigorous introduction, consult Ref. [15].

2.4 Statistical physics

The number of particles in a macroscopic system is usually tremendously high. For example, in one mole of water there is about $6.022 \cdot 10^{23}$ (Avogadro's number) H_2O molecules, and that only amounts to about 18 ml. In order to describe the physical macroscopic properties of such a system, one cannot simply go ahead and solve all the equations of motion for each particle. Instead, one can describe the system in a probabilistic way, by defining the *partition function*,

$$\mathcal{Z} = \sum_{\{\Psi\}} \mathrm{e}^{-\beta H_\Psi} \,. \tag{2.17}$$

Here, H_Ψ is the Hamiltonian of the system in a given configuration Ψ, and $\beta = 1/k_\mathrm{B}T$. The partition function therefore represents a weighted sum over all possible states of the system. In fact, all relevant thermodynamical quantities are contained in $\mathcal{Z}$, and we can obtain the expectation values for any observable O of the system through the relation

$$\langle O \rangle = \frac{1}{\mathcal{Z}} \sum_{\{\Psi\}} O_\Psi \, \mathrm{e}^{-\beta H_\Psi} \,. \tag{2.18}$$

$\mathcal{Z}$ therefore also serves as a normalization factor. All thermodynamical quantities can now be derived, such as the internal energy $U \equiv \langle H \rangle = -(\partial/\partial\beta) \ln \mathcal{Z}$, Helmholtz free energy $F = -k_\mathrm{B}T \ln \mathcal{Z}$ and the heat capacity $C_V = -k_\mathrm{B}\beta^2(\partial^2/\partial\beta^2) \ln \mathcal{Z}$.[4]

Statistical physics is therefore a framework that connects the observable macroscopic properties with the underlying microscopic structure of the system.

The heat capacity C_V can also be expressed through the energy fluctuations in the system,

$$C_V = k_\mathrm{B}\beta^2 \left\langle (H - \langle H \rangle)^2 \right\rangle = k_\mathrm{B}\beta^2 \left(\langle H^2 \rangle - \langle H \rangle^2 \right) , \tag{2.19}$$

[4] The specific heat is given by $c_V = C_V/\rho V$, where ρ is the mass density and $V = L^d$ is the volume of the d dimensional system.

or simply $C_V = k_B \beta^2 \mu_2^H$, where μ_n^X is the n'th moment of the variable X. One important feature of the heat capacity, is that it tends to diverge at a phase transition, as the energy fluctuations go haywire; the competition between the ordered and disordered phase is at its maximum. We say that the system is in a *critical* state, and that we study critical phenomena. A good introduction is given in Ref. [16].

2.4.1 Broken symmetries and phase transitions

As we have seen in the previous sections, a many-particle system is usually described by a Hamiltonian H. Now, if the energy H_Ψ remains unchanged under some transformation of the microscopic state Ψ, we say that the *system* is *symmetric* or *invariant* under that transformation.

This notion of symmetry can be illustrated using the Ising-model, which is rich in features despite its simple Hamiltonian. It will be used to illustrate some concepts in the following.

In 1925 Ernst Ising solved a model of interacting spins on a one-dimensional chain [17]. The model, which today bears his name, describes a very simple ferromagnet. The Ising-Hamiltonian reads

$$H_{\text{Ising}} = -J \sum_{\langle i,j \rangle} \sigma_i \sigma_j - h \sum_i \sigma_i, \tag{2.20}$$

where $\sigma_i = \pm 1 = \uparrow, \downarrow$ represent spin up or spin down for particle i, and the first sum goes over all nearest neighbors of such spins, and the second sum goes over all N spins. The coupling constant J is assumed to be positive, so that in order to minimize the internal energy, the spins will tend to point in the same direction[5]. In the last term, h corresponds to an external magnetic field, that will force the spins to point in a given direction depending on the sign of h. Let us first consider the case when $h = 0$, *i.e.* the Ising-model in zero magnetic field. Clearly, in this case, the sum in (2.20) is unchanged under the transformation $\sigma_i \to -\sigma_i$ (for all i), and we say that it has a Z_2 symmetry. If we look at the magnetization,

$$M_\sigma = \frac{1}{N} \sum_i \sigma_i, \tag{2.21}$$

which serves as an *order parameter*, we see that this quantity does not necessarily have the same symmetry. At high temperatures, in the disordered phase, the spins are fluctuating randomly between pointing up or down. Consequently, the magnetization will be zero at

[5] In general, the Helmholz free energy $F = U(T) - TS(T)$ is minimized, where $U = \langle H \rangle$, and S is the entropy of the system. For high temperatures T, the internal energy U becomes irrelevant and the system tends to reach a higher entropy, whereas for low temperatures, the internal energy U is minimized since the last term becomes negligible.

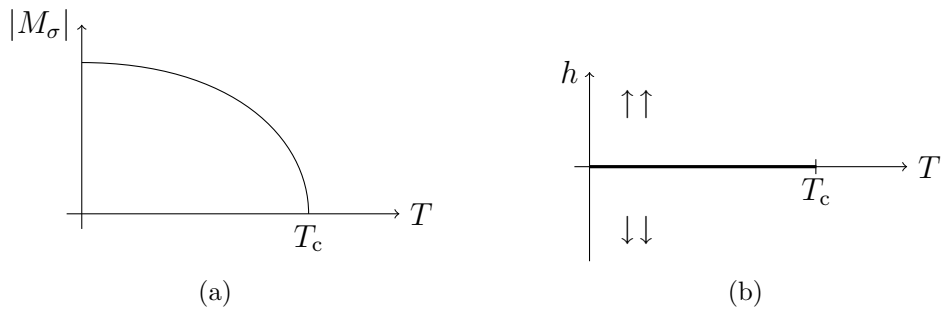

(a) (b)

Figure 2.2: (a) The magnetization M_σ goes continuously to zero at $T = T_c$ when the temperature is increased. (b) At $h = 0$, the thick line indicates a non-zero magnetization M_σ, taking the value $+1$ or -1. For $T < T_c$, if the external magnetic field h is increased from 0^- to 0^+, the magnetization will undergo a first order transition.

high temperatures. However, if all the spins were to point in one direction, the magnetization would be plus or minus one. When (if) the system enters this ordered phase, the symmetry is *spontaneously broken*, *i.e.* the state Ψ does no longer possess the symmetry of the Hamiltonian H.

As Ising showed in 1925, in no external field ($h = 0$), a one-dimensional chain of Ising-spins does not have any phase transition for $T > 0$. The model does, however, have temperature driven phase transitions in higher dimensions, *e.g.* for $d = 2$. In 1944 Lars Onsager showed this by giving the exact solution of the Ising-model in two dimensions with no external field[6] [18]. From his paper, one can derive the analytical expression for the critical inverse temperature for an isotropic Ising-model, namely $\beta_c = \ln(1 + \sqrt{2})/2 \simeq 0.44$ (or $T_c \simeq 2.27$) when $J = 1$, $k_B = 1$.

So, for $d = 2$, the Ising-model has a temperature driven phase transition from a disordered phase at high temperatures, to an ordered phase for $T < T_c$. This transition is *continuous*, *i.e.* the magnetization in (2.21) goes continuously to zero when $T \to T_c^-$, see Figure 2.2(a). If we turn on the external field by letting $h > 0$, and look at the system in the ordered phase ($T < T_c$), we expect all spins to point upwards, as that would minimize the energy in (2.20). Now, if we keep the temperature fixed, but gently decrease the field h to a negative value, we will notice an abrupt change in the system—all spins will flip and point downwards. This transition is clearly not continuous, and is called a *first order* phase transition.

In the above we have seen that the two-dimensional Ising-model has both a continuous and a first order phase transition, depending on the path in parameter space that is used, in this case T or h.

[6] In fact, he considered an anisotropic Ising-model, where the interaction was different in the x- and y-directions.

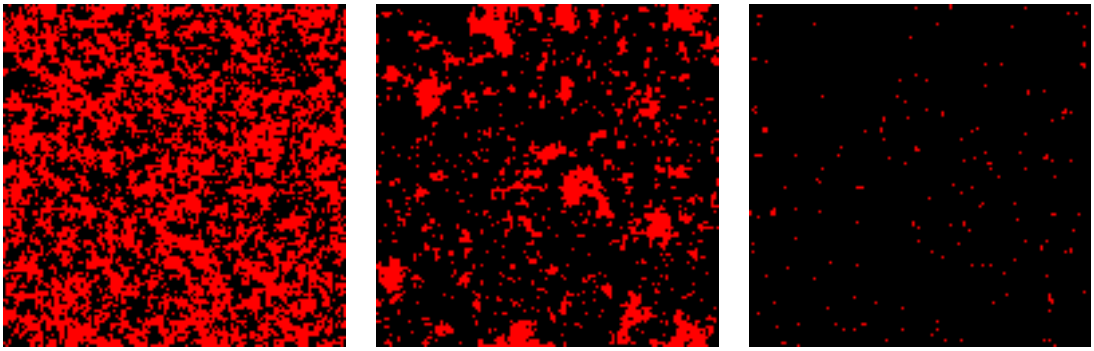

(a) (b) (c)

Figure 2.3: Snapshots of an isotropic Ising model in two dimensions on a 128×128 grid, computed using Monte Carlo simulations. (a) At high temperatures the spins are randomly distributed between $\uparrow$ (red) and $\downarrow$ (black). (b) Near the critical temperature $T_c \simeq 2.27$ ($\beta_c \simeq 0.44$, $J = 1$). (c) At low temperature, almost all spins point in the same direction—in this case down.

In Figure 2.3 we see three snapshots of the continuous temperature driven phase transition for the 2D Ising-model, based on a Monte Carlo simulation of a 128×128 grid of spins.

2.5 Mean field approximation

When studying many-particle physics analytically, one is challenged by how to treat the interaction term in the Hamiltonian when summing over all states. This boils down to a combinatorial challenge when one tries to account for the symmetries of the problem. When each particle in the system depends on all other particles, this is obviously an impractical task. Even when only nearest neighbors are considered, it is convenient to convert the two-particle interactions into a one-body problem. One way to do this is to apply the *mean field approximation*.

If we turn to the Ising-model (2.20) and look at the interaction term there, we can express the spin at site i by its deviation from the mean value, *i.e.*

$$\sigma_i = \langle \sigma_i \rangle + \delta\sigma_i, \tag{2.22}$$

where we have defined $\delta\sigma_i = \sigma_i - \langle\sigma_i\rangle$. Now, if we insert this in (2.20), we get

$$\begin{aligned} H_{\text{Ising}}^{\text{MF}} &= -J \sum_{\langle i,j\rangle} \left(\langle\sigma_i\rangle + \delta\sigma_i\right)\left(\langle\sigma_j\rangle + \delta\sigma_j\right) \\ &= -J \sum_{\langle i,j\rangle} \left(M_\sigma(\sigma_i + \sigma_j) - M_\sigma^2\right) + \mathcal{O}(\delta\sigma)^2 \\ &\simeq JzNM_\sigma^2 - 2JzM_\sigma \sum_i \sigma_i, \end{aligned} \tag{2.23}$$

where we have used that $M_\sigma = \langle\sigma_i\rangle$ (2.21) and that each lattice point has got $z = 2d$ nearest neighbor points, where d is the spatial dimension of the problem. This way, the two-particle problem has been reduced to a single-particle problem, but the coupling constant is now accompanied by the mean value of the sum variable.

As already mentioned, Ising and Onsager have solved the model *exactly* without using the mean field approximation. In fact, if one tries to extract critical exponents or even the critical temperature using the mean field approximation in $d = 1$, the results will be wrong. For example, if we insert (2.23) in (2.17) and calculate the magnetization self-consistently, we find that there should be a phase transition at $\beta_c = 1/2Jz$, which is not the case in one dimension.

Nevertheless, we will see later that the mean field approximation proves to be useful, especially for second-quantized Hamiltonians describing systems far away from the critical temperature.

2.6 Monte Carlo simulations

We saw in Section 2.4 that in order to calculate the expectation value of an observable quantity one can use the partition function and evaluate (2.18). For example, the heat capacity could be obtained through $\mathcal{Z}$. However, in order to actually calculate $\mathcal{Z}$, one has to sum over all possible states, see (2.17). If we again turn to the 2D Ising-model, and consider a 10×10 grid, we find that we have $2^{100} \simeq 10^{30}$ possible states. In the thermodynamical limit, when $V = L^2 \to \infty$, this direct approach is therefore not applicable. Instead, one can use the *Monte Carlo method*.

For starters, let us look at a simple example in order to grasp the essence of what Monte Carlo is. Say you want to calculate the number π, *i.e.* the ratio of a circle's circumference to its diameter. Imagine yourself on the beach. Draw a perfect square in the sand, and inscribe a perfect circle in it.[7] Now, toss a number of small stones into the square (in a

[7] Take this as a "Gedankenexperiment". For a real life experiment, consider using a square and a circular bucket outside on a rainy day.

perfectly uniform manner). Then count the total number of stones inside the square N_{square} and the fraction of stones inside the circle N_{circle}. Since the areas are given by $A_{\text{square}} = 4r^2$ and $A_{\text{circle}} = \pi r^2$, we can estimate the value of π by

$$\pi = 4\frac{A_{\text{circle}}}{A_{\text{square}}} \simeq 4\frac{N_{\text{circle}}}{N_{\text{square}}}. \tag{2.24}$$

If you do this with ~ 10000 stones inside the square, you will find π to be around 3.14. If you want to increase the accuracy, you can keep on tossing stones until you reach the accuracy you want.

Now, this is certainly not the best way to calculate π, but it illustrates how one can use randomness to achieve accurate results, *i.e. randomness does not imply inaccuracy.* The name "Monte Carlo" is just a slang term for "statistical sampling", with references to a famous casino in Monaco.

Importance sampling

The plots showing snapshots of the magnetization in Section 2.4.1 were calculated using Monte Carlo simulations. As a thermodynamical system, the ordering is governed by the partition function (2.17), because the system tends to minimize the Helmholtz free energy. This is done by "choosing" the states Ψ that do exactly that. Now, since only relatively few states contribute to the sum in the partition function (2.17), it makes sense to focus on those. According to the central limit theorem, the expectation value in (2.18) can be estimated by the average

$$\langle O \rangle \simeq \frac{1}{N}\sum_{\alpha=1}^{N} O(\Psi_\alpha), \tag{2.25}$$

if the N states Ψ_α are picked out independently with a probability given by

$$p(\Psi_\alpha) = \frac{\mathrm{e}^{-\beta H(\Psi_\alpha)}}{\mathcal{Z}}, \tag{2.26}$$

known as the Boltzmann probability.

This way, it is more probable to pick out states that are thermodynamically close. Consequently, one is ensured that the system spends most of the time in a state $H(\Psi) \simeq \langle H \rangle$, so that time wasted on states that do not contribute much to the sum is at a minimum.

So instead of making a random sampling of the states Ψ, we use *importance sampling*, where only the most important states are considered.

Markov chain

In order to pick out the important states independently according to the Boltzmann probability in (2.26), we need a way to generate a new state $\Psi_{\alpha'}$ from the current state Ψ_α in a random fashion. A process where the new state does not depend on any other states but the previous one, is called a Markov process. If we introduce the transition probability $P(\Psi_\alpha \to \Psi_{\alpha'})$ with the accompanying normalization $\sum_{\{\alpha'\}} P(\Psi_\alpha \to \Psi_{\alpha'}) = 1$, there are two more important requirements associated with the Markov process. First, we must be sure that it is possible to reach the full phase space, *i.e.* that if we start out in any given state Ψ_{α_0}, the system can evolve to any state $\Psi_{\alpha'}$ in a *finite number of steps*. We can call this *accessibility*[8]. Furthermore, at equilibrium, a *detailed balance* must be fulfilled, namely

$$p(\Psi_\alpha)P(\Psi_\alpha \to \Psi_{\alpha'}) = p(\Psi_{\alpha'})P(\Psi_{\alpha'} \to \Psi_\alpha), \tag{2.27}$$

which states that the rate at which a system in state Ψ_α goes to a state $\Psi_{\alpha'}$, is the same as the rate of the opposite transition.

A Monte Carlo simulation constitutes a series of such random transitions, and we call it the *Markov chain*. The transition probability $P(\Psi_\alpha \to \Psi_{\alpha'})$ is yet undefined, but from the detailed balance (2.27) we find that

$$\frac{P(\Psi_\alpha \to \Psi_{\alpha'})}{P(\Psi_{\alpha'} \to \Psi_\alpha)} = \frac{p(\Psi_{\alpha'})}{p(\Psi_\alpha)} = \mathrm{e}^{-\beta(H(\Psi_{\alpha'})-H(\Psi_\alpha))} \equiv \mathrm{e}^{-\beta\Delta H}\,. \tag{2.28}$$

Thus, we are left with some freedom in how we choose the transition probabilities. We will consider one way of doing it, known as the *Metropolis algorithm*.

Metropolis–Hastings algorithm

In 1953 Metropolis *et al.* [19] gave a description of how to produce a set of Boltzmann distributed variables from a set of random numbers. This is exactly what is needed in order to implement the Markov chain described above on a computer. The method was later generalized by Hastings [20], and is known as the Metropolis–Hastings algorithm, but is often referred to simply as the Metropolis algorithm. Although the method is not the only one possible that satisfies (2.28), it is simple, convenient and "does the job".

The Metropolis algorithm brings the system from an initial state Ψ_0 to the next state in consecutive steps. It can be described by the following set of rules:

0. Generate the initial state $\Psi_\alpha = \Psi_0$.

[8] It is also often referred to as *ergodicity*, which means that at equilibrium, all states with the same energy are equally probable, which also implies that they can all be reached.

1. Generate a new state $\Psi_{\alpha'}$ randomly.

2. Calculate $\Delta H = H(\Psi_{\alpha'}) - H(\Psi_\alpha)$.

3. Accept the new state with probability $P = \min(1, \mathrm{e}^{-\beta\Delta H})$.
   In other words: Draw a random number $r \in [0, 1]$ from a uniform distribution, and accept the new configuration if[9] $r < P$.

4. Make measurements on the state.

5. Repeat step 1 to 4 until the accuracy required is reached.

These rules constitute the core of the Monte Carlo simulation, and will after (usually) several thousand iterations bring the system into an equilibrium where the next iteration will keep the system in the same ensemble. It is easy to see that the detailed balance in Eq. (2.27) is fulfilled, as

$$\frac{P(\Psi_\alpha \to \Psi_{\alpha'})}{P(\Psi_{\alpha'} \to \Psi_\alpha)} = \frac{\min(1, \mathrm{e}^{-\beta\Delta H})}{\min(1, \mathrm{e}^{\beta\Delta H})} = \left\{ \begin{array}{lll} \frac{1}{\mathrm{e}^{\beta\Delta H}} & \text{for} & \Delta H \leq 0 \\ \frac{\mathrm{e}^{-\beta\Delta H}}{1} & \text{for} & \Delta H \geq 0 \end{array} \right\} = \frac{p(\Psi_{\alpha'})}{p(\Psi_\alpha)}. \tag{2.29}$$

Note that in step 3 above, the new state is always accepted if it leads to a lowering of the energy, which is the physical driving force.

2.6.1 Critical slowing down

Since the Metropolis algorithm evaluates the energy of the system at a given temperature and accepts or rejects the new state based on the change in energy in a temperature-dependent way, it is more likely to accept new states at high temperatures compared to low temperatures. Also, since the new configuration depends on the previous configuration, we find that near the phase-transition, when the system is highly correlated, updates are less likely. The simulation is therefore said to suffer from *critical slowing down*.

This affects the errors in the variables one wants to measure, as consecutive states are not really independent. One way to deal with this is to increase the number of Monte Carlo sweeps, which of course means more CPU hours. Alternatively, one can turn to other, non-local update methods, often referred to as *cluster methods*. The Swendsen–Wang algorithm [21] is one example of a cluster algorithm.

[9] Equivalently, we can test for $r < \mathrm{e}^{-\beta\Delta H}$. In the actual code, we prepare a list of random numbers $R = \ln(r)/\beta$ and check if $R < -\Delta H$.

2.6.2 Critical exponents and finite size scaling

When doing Monte Carlo simulations, we are ultimately interested the behavior in the thermodynamical limit, *i.e.* when $L \to \infty$. Specifically, we try to find the critical temperature and the *critical exponents* of the system. As mentioned in Section 2.4, at the phase transition the system is in a critical state. This is reflected in the thermodynamical quantities by non-analyticies at $T = T_c$. The strength of this divergence is given by the critical exponents, conventionally denoted α, β, γ, ν where the heat capacity $C_V \sim |T - T_c|^{-\alpha}$, the magnetization $M \sim (T_c - T)^{\beta}$, the magnetic susceptibility $\chi \sim |T - T_c|^{-\gamma}$, and the correlation length $\xi \sim |T - T_c|^{-\nu}$, just to mention a few.

Since we can only consider systems of finite size in our computer simulations, we will not see this singular behavior in the thermodynamical quantities. The divergences will be finite, and the critical temperature may be shifted. This is known as *finite size effects*. But since it is possible to do the simulations on various system sizes, we can still extract the true critical behavior by treating the results for different L values systematically. This is known as *finite size scaling*. What one usually does, is to consider the correlation length mentioned above, which is a measure of the range over which fluctuations in one region is correlated with those in another region. At the critical point, this quantity is known to diverge, *i.e.* the whole system is correlated. Since any measure of length in a finite system is confined by the system size, we expect that $\xi \to L$ as $T \to T_c$. This implies that $|T - T_c| \sim L^{-1/\nu}$ near T_c.

If we transfer this to the other quantities, we find that *e.g.* $\chi \sim L^{\gamma/\nu}$. Thus, by measuring the height of the peak in the susceptibility for various system sizes L, we can extract the ratio γ/ν of the critical exponents. Similarly, one can consider the so-called *Binder ratio* or *Binder cumulant* for the magnetization [22, 23],

$$G_L = \frac{\langle \boldsymbol{m}^4 \rangle_L}{\langle \boldsymbol{m}^2 \rangle_L^2}, \tag{2.30}$$

where $\boldsymbol{m}$ is the magnetization vector of the system, $\boldsymbol{m}^2 = \boldsymbol{m} \cdot \boldsymbol{m}$. This (dimensionless) function has the property that when it is plotted as a function of temperature, all data for different system sizes L will intersect at the critical temperature. Moreover, if it is plotted as a function of $L^{1/\nu}(T - T_c)/T_c$, one can find the critical exponent ν by tuning it until *data collapse* [24] occur. Details on finite size effects and scaling can be found in *e.g.* Refs. [23, 25].

3 Building blocks

In Paper I, II and III [1, 2, 3] we have studied quantum transport in systems that has one or more broken symmetries. That is, the systems under consideration have *ferromagnetic order*, *superconducting order* or *spin-orbit coupling* present—or they possess a *combination* of these properties. These papers will be introduced in Chapter 4. In Paper IV [4], which will be introduced in Chapter 5, we have studied high-T_c superconductors in the non-superconducting state.

In this chapter, the core ingredients mentioned above are introduced separately, so that the various combinations that will be discussed in Chapter 4 have a common base for reference. Natural units are used, $\hbar = k_B = 1$.

3.1 Ferromagnetism

Of all the phenomena that are due to cooperative electronic behavior, the macroscopic effect called magnetism is maybe the longest known. The attractive force of magnetite was reported by the Greeks some 2800 years ago. In daily language, when we talk about *magnets*, we usually refer to *ferrimagnetism* or *ferromagnetism*, simply because permanent magnets are either ferrimagnetic or ferromagnetic. A ferrimagnet has got anti-ferromagnetic ordering between the sublattices, but the opposing magnetic moments of each sublattice are unequal, so that the material as a whole is magnetized. Magnetite (Fe_3O_4) is in fact a ferrimagnet. Pure Iron (Fe), however, is a ferromagnet.

A *ferromagnet* is a material where all the magnetic moments in the lattice tend to point in the same direction. Atoms with partially filled shells can experience a net magnetic moment in the absence of an external field, due to unpaired spins. These spins can be aligned when the material is exposed to an external magnetic field, and can cause the material to be spontaneously magnetized and carry a net magnetic moment for some time,

even when it is no longer in the external field.

Theory

In the following, we will deal with ferromagnets. They can be described by the so-called Heisenberg Hamiltonian, where the spins of each lattice site interact via a vector interaction. If we only consider nearest neighbors in the interaction and assume the interaction to be isotropic, it reads

$$H_{\mathrm{FM}} = -J \sum_{\langle i,j \rangle} \boldsymbol{S}_i \cdot \boldsymbol{S}_j, \tag{3.1}$$

where J is the (isotropic) coupling constant, $\boldsymbol{S}_i = (1/2) \sum_{\alpha\beta} c^\dagger_{i\alpha} \hat{\boldsymbol{\sigma}}_{\alpha\beta} c_{i\beta}$ is the spin operator, in which $\{\alpha, \beta\} \in \pm 1$ are spin indices and $\hat{\boldsymbol{\sigma}}$ is a vector containing the Pauli matrices[1]. The brackets $\langle \cdot, \cdot \rangle$ in the sum indicates that only nearest neighbors should be considered. This can be cast into a momentum space representation, where it reads

$$H_{\mathrm{FM}} = -JN \sum_{\boldsymbol{k}} \eta(\boldsymbol{k}) \boldsymbol{S}_{\boldsymbol{k}} \cdot \boldsymbol{S}_{-\boldsymbol{k}}. \tag{3.2}$$

Here, N is the number of particles, $\eta(\boldsymbol{k})$ is a geometrical structure factor which for $\boldsymbol{k} = 0$ reduces to the number of nearest lattice neighbors; $\eta(0) = 4$ in two dimensions, and the spin operator $\boldsymbol{S}_{\boldsymbol{k}} = (1/2) \sum_{\alpha\beta} c^\dagger_{\boldsymbol{k}\alpha} \hat{\boldsymbol{\sigma}}_{\alpha\beta} c_{\boldsymbol{k}\beta}$.

If we compare (3.1) with the simple classical Ising version in (2.20) (in zero field, $h = 0$), we see that we now have a second quantized version where the spins can point in an arbitrary direction.

We will take the $\boldsymbol{k} = 0$ component of the spin operator, to reflect the bulk global ferromagnetic order. Then, on the mean field level, we find

$$H_{\mathrm{FM}} = H_0^{\mathrm{FM}} + \sum_{\boldsymbol{k}} \phi^\dagger_{\boldsymbol{k}} \hat{A}^{\mathrm{FM}}_{\boldsymbol{k}} \phi_{\boldsymbol{k}}, \tag{3.3a}$$

where the basis $\phi_{\boldsymbol{k}} = (c_{\boldsymbol{k}\uparrow}, c_{\boldsymbol{k}\downarrow})^{\mathrm{T}}$ and

$$\hat{A}^{\mathrm{FM}}_{\boldsymbol{k}} = -\begin{pmatrix} \zeta_z & \zeta_{xy} \\ \zeta^\dagger_{xy} & -\zeta_z \end{pmatrix} = -\boldsymbol{\zeta} \cdot \hat{\boldsymbol{\sigma}} \tag{3.3b}$$

$$\begin{aligned} \zeta_z &= 2J\eta(0) m_z \\ \zeta_{xy} &= 2J\eta(0)(m_x - \mathrm{i} m_y). \end{aligned} \tag{3.3c}$$

[1] $\hat{\boldsymbol{\sigma}} = (\hat{\sigma}_1, \hat{\sigma}_2, \hat{\sigma}_3)$, with $\hat{\sigma}_1 = \begin{pmatrix} 0 & 1 \\ 1 & 0 \end{pmatrix}$, $\hat{\sigma}_2 = \begin{pmatrix} 0 & -\mathrm{i} \\ \mathrm{i} & 0 \end{pmatrix}$, $\hat{\sigma}_3 = \begin{pmatrix} 1 & 0 \\ 0 & -1 \end{pmatrix}$. Also, let $\hat{\sigma}_0 = \begin{pmatrix} 1 & 0 \\ 0 & 1 \end{pmatrix}$.

The magnetization is given by $\boldsymbol{m} = (m_x, m_y, m_z) = (1/N)\sum_i \langle \boldsymbol{S}_i \rangle = \langle \boldsymbol{S}_{\boldsymbol{k}=0} \rangle$ in the isotropic case that we are studying, and $H_0^{\mathrm{FM}} = J\eta(0)\boldsymbol{m}^2$.

In its present form, Eq. (3.3) is suitable for combination with other Hamiltonians, as we will see in the following.

3.2 Superconductivity

In the previous section we looked at collective electron interactions that led to the macroscopic phenomenon called ferromagnetism. *Superconductivity* is also due to collective electron interactions, although of a much more sophisticated nature. It was discovered experimentally by Heike Kamerlingh Onnes and co-workers in 1911 [26]. They found that the electrical resistivity of mercury (Hg) dropped to zero near the extremely low temperature of 4 K (−269°C).

Another remarkable property was discovered by Meissner and Ochsenfeld in 1933 [27]—perfect diamagnetism. That is, a superconducting material in its superconducting state, will expel a magnetic field as long as it its strength is below some threshold[2]. It is know as the Meissner effect.

The materials described here, are now known as type-I superconductors, and can be characterized by the following two hallmarks:

- Perfect DC conductivity at temperatures below the critical temperature T_{c}.
- Perfect diamagnetism below the critical temperature T_{c}.

Examples of type-I superconductors are aluminum, (Al), lead (Pb), tin (Sn) and niobium (Nb). A comprehensive introduction to superconductivity can be found in Ref. [28].

3.2.1 Type-I and type-II superconductors

The temperatures needed for type-I superconductivity were all extremely low, and required liquid helium for cooling, which is rather expensive. When Bednorz and Müller in 1986 discovered high-temperature superconductivity [29], one was quickly able to use the much cheaper coolant liquid nitrogen. Bednorz and Müller established the existence of superconductivity in a Ba doped La-Cu-O compound at about 30 K (−243°C)—the highest critical

[2] Actually, even for a conventional type-I superconductor, the magnetic field will penetrate into the material by a small distance λ, called the *London penetration depth*. For bulk superconductors λ is usually less than a few hundreds nm.

temperature till then. Shortly after, a Y-Ba-Cu-O compound was found to be superconducting at around 90 K (−183°C), well above the boiling point of liquid nitrogen (77 K) [30]. Bednorz and Müller were awarded the Nobel Prize in 1987 [31] for their discovery.

The materials in this new group of superconductors are, of course, also perfect conductors below a critical temperature T_c, but their response to an externally applied magnetic field is radically different. Whereas a type-I superconductor will revert to the normal phase if the external magnetic field H exceeds a critical limit H_c, a type-II superconductor will first enter an intermediate phase for $H_{c_1} < H < H_{c_2}$. In this phase an Abrikosov flux lattice will form [32]. This state is often called the mixed state. When $H > H_{c_2}$ a type-II superconductor will also return to the normal state. In the mean field scheme, where fluctuations are neglected, the classification of type-I and type-II superconductors can be based on the relative magnitude of the magnetic penetration depth λ (typical radius of a vortex) and the coherence length ξ (typical size of a Cooper-pair). The Ginzburg-Landau parameter $\kappa = \lambda/\xi$ predicts a type-I superconductor for $\kappa < 1/\sqrt{2}$ and a type-II for $\kappa > 1/\sqrt{2}$. This prediction is based a sign-change in the surface energy associated with the applied magnetic field, which for a type-II superconductor it is energetically favorable to maximize the surface, and thus allows for flux penetration [28].

Today, superconductors play a central role in for example magnetic resonance imaging (MRI), which makes use of nuclear magnetic resonance (NMR) in order to visualize structures inside a patient's body[3]. In order to build up the strong magnetic field needed to do MRI, superconducting electromagnets are used, typically a type-II superconductor, *e.g.* niobium-titanium, NiTi.[4]

3.2.2 Theory of type-I superconductivity

A microscopic theory of type-I superconductivity was provided by John Bardeen, Leon Nathan Cooper and John Robert Schrieffer in 1957, the so-called BCS-theory [33]. Although the results in the BCS theory does not depend on the origin the attractive interaction that leads to Cooper-pairs, it is on most cases phonon-mediated in conventional superconductors. In other terms, the attractive interaction between two electrons is an indirect consequence of how the electrons interact with the atomic lattice. If we consider an electron that moves through the material, it will attract positive charges in the lattice and thus deform the lattice and leave a trace. Another electron will be attracted by the increased positive charge density and move in the opposite direction. Effectively, these two electrons are held together (in momentum space) by a certain binding energy that will be higher than any interaction with the (vibrating) lattice—provided that the temperature

[3] MRI was formerly known as NMRI: Nuclear Magnetic Resonance Imaging, but was rephrased to MRI because of negative associations with the word "nuclear".

[4] NiTi is in fact a metallic type-II superconductor, as opposed to most type-II superconductors, that are either isolators or poor conductors.

is low enough. This way the electron pair, *i.e.* the Cooper-pair, will not experience any resistance at $T < T_c$.

Leon Cooper was the first to show [34] how an arbitrarily small attraction between two electrons could lead to a paired state with an energy lower than the Fermi energy. If we let many electrons form pairs, one finds that there opens up a gap in the continuous energy spectrum of allowed energy states for the fermions. This means that there will be a minimum amount of energy needed to break the Cooper-pairs, and thus that small excitations such as scattering is forbidden, which is just yet another way of saying that resistivity is lost below T_c. Bardeen, Cooper and Schrieffer received the Nobel prize for the BCS-theory in 1972 [35].

Hamiltonian

If we generalize the original BCS Hamiltonian [33] to also account for spin-triplet pairing, it can be written as

$$H_{\mathrm{SC}} = \sum_{\boldsymbol{k}\alpha} (\varepsilon_{\boldsymbol{k}} - \mu) c^\dagger_{\boldsymbol{k}\alpha} c_{\boldsymbol{k}\alpha} + \frac{1}{2} \sum_{\boldsymbol{k}\boldsymbol{k}'\alpha\beta} V_{\boldsymbol{k}\boldsymbol{k}'\alpha\beta} c^\dagger_{\boldsymbol{k}\alpha} c^\dagger_{-\boldsymbol{k}\beta} c_{-\boldsymbol{k}'\beta} c_{\boldsymbol{k}'\alpha}, \tag{3.4}$$

where α and β are spin indices, and $V_{\boldsymbol{k}\boldsymbol{k}'\alpha\beta}$ is an effective electron-electron interaction giving rise to Cooper-pairing. The chemical potential is denoted μ, and $c^\dagger_{\boldsymbol{k}\sigma}$ ($c_{\boldsymbol{k}\sigma}$) creates (annihilates) a fermion in state $\boldsymbol{k}$ with spin σ.[5] If we apply the mean field approximation[6], we cast this into

$$H_{\mathrm{SC}} = \sum_{\boldsymbol{k}\alpha} (\varepsilon_{\boldsymbol{k}} - \mu) c^\dagger_{\boldsymbol{k}\alpha} c_{\boldsymbol{k}\alpha} - \frac{1}{2} \sum_{\boldsymbol{k}\alpha\beta} \left[\Delta^\dagger_{\boldsymbol{k}\alpha\beta} c_{-\boldsymbol{k}\beta} c_{\boldsymbol{k}\alpha} + \Delta_{\boldsymbol{k}\alpha\beta} c^\dagger_{\boldsymbol{k}\alpha} c^\dagger_{-\boldsymbol{k}\beta} - \Delta^\dagger_{\boldsymbol{k}\alpha\beta} b_{\boldsymbol{k}\alpha\beta} \right], \tag{3.5}$$

where $b_{\boldsymbol{k}\alpha\beta} = \langle c_{-\boldsymbol{k}\beta} c_{\boldsymbol{k}\alpha} \rangle$ is the two particle expectation value, and the order parameter $\Delta_{\boldsymbol{k}'\alpha\beta} = -\sum_{\boldsymbol{k}} V_{\boldsymbol{k}\boldsymbol{k}'\alpha\beta} b_{\boldsymbol{k}\alpha\beta}$. In matrix form we have

$$H_{\mathrm{SC}} = H_0^{\mathrm{SC}} - \frac{1}{2} \sum_{\boldsymbol{k}} \varphi^\dagger_{\boldsymbol{k}} \check{\Delta}_{\boldsymbol{k}} \varphi_{\boldsymbol{k}}, \tag{3.6a}$$

[5] The conventional spin-singlet BCS Hamiltonian is regained by letting $\beta \to -\alpha$.

[6] One way of justifying the mean field approximation here, is by looking at (3.4) as an analogue to a ferromagnet, for details see Ref. [28].

where the basis $\varphi_{\boldsymbol{k}} = (\phi_{\boldsymbol{k}}, \phi^{\dagger\mathrm{T}}_{-\boldsymbol{k}})^{\mathrm{T}} = (c_{\boldsymbol{k}\uparrow}, c_{\boldsymbol{k}\downarrow}, c^{\dagger}_{-\boldsymbol{k}\uparrow}, c^{\dagger}_{-\boldsymbol{k}\downarrow})^{\mathrm{T}}$, and

$$\check{\Delta}_{\boldsymbol{k}} = \begin{pmatrix} 0 & \hat{\Delta}_{\boldsymbol{k}} \\ \hat{\Delta}^{\dagger}_{\boldsymbol{k}} & 0 \end{pmatrix}, \tag{3.6b}$$

$$\hat{\Delta}_{\boldsymbol{k}} = \begin{pmatrix} \Delta_{\boldsymbol{k}\uparrow\uparrow} & \Delta_{\boldsymbol{k}\uparrow\downarrow} \\ \Delta_{\boldsymbol{k}\downarrow\uparrow} & \Delta_{\boldsymbol{k}\downarrow\downarrow} \end{pmatrix} = \mathrm{i}(\boldsymbol{d}_{\boldsymbol{k}} \cdot \hat{\boldsymbol{\sigma}} + d^0_{\boldsymbol{k}})\sigma_y \tag{3.6c}$$

$$d^0_{\boldsymbol{k}} = \frac{1}{2}(\Delta_{\boldsymbol{k}\uparrow\downarrow} - \Delta_{\boldsymbol{k}\downarrow\uparrow}) \tag{3.6d}$$

$$\boldsymbol{d}_{\boldsymbol{k}} = \left(-\tfrac{1}{2}(\Delta_{\boldsymbol{k}\uparrow\uparrow} - \Delta_{\boldsymbol{k}\downarrow\downarrow}), -\tfrac{\mathrm{i}}{2}(\Delta_{\boldsymbol{k}\uparrow\uparrow} + \Delta_{\boldsymbol{k}\downarrow\downarrow}), \tfrac{1}{2}(\Delta_{\boldsymbol{k}\uparrow\downarrow} + \Delta_{\boldsymbol{k}\downarrow\uparrow})\right). \tag{3.6e}$$

Also, $H_0^{\mathrm{SC}} = \sum_{\boldsymbol{k}\alpha\beta}[(\varepsilon_{\boldsymbol{k}} - \mu)c^{\dagger}_{\boldsymbol{k}\alpha}c_{\boldsymbol{k}\alpha}\delta_{\alpha\beta} + \Delta^{\dagger}_{\boldsymbol{k}\alpha\beta}b_{\boldsymbol{k}\alpha\beta}]/2$. The $\boldsymbol{d}$-vector formalism [36] introduced above is convenient for categorizing the spin-triplet state, and allows for a more compact representation of the energy spectrum. Here, and in the rest of this chapter, $\check{m}$ denotes a 4×4 matrix, and $\hat{m}$ denotes a 2×2 matrix.

Note that the Hamiltonians in Eqs. 3.4 and 3.5 are $U(1)$ symmetric, *i.e.* they remain unchanged under the transformation $c_{\boldsymbol{k}\sigma} \to c_{\boldsymbol{k}\sigma}\, \mathrm{e}^{\mathrm{i}\theta/2}$. At the critical temperature, T_{c}, *when the Cooper-pairs condense*, the phase of the gap function $\Delta_{\boldsymbol{k}\alpha\beta}$ will freeze in such a way that the macroscopic system acquires a global phase, *i.e.* the $U(1)$ symmetry is lost.

3.2.3 Pairing symmetry

Electrons are spin-1/2 particles so the total spin of a Cooper-pair can be either $S = 0$ (singlet) or $S = 1$ (triplet). The total wave function of the Cooper-pair should be anti-symmetric under interchange of the fermions, due to the Pauli principle. Thus, provided that the wave function factorizes into a spatial part and a spin part, which is usually the case, the orbital part of the wave function for spin-singlet is symmetric ($l = 0$; s-wave, $l = 2$; d-wave, etc.), and that for the spin-triplet it is anti-symmetric ($l = 1$; p-wave, etc.). From (3.6d) we see that, with regard to spin, $d^0_{\boldsymbol{k}}$ is anti-symmetric and corresponds to a spin-singlet, with symmetric spatial part, *e.g.* s-wave, and that $\boldsymbol{d}_{\boldsymbol{k}}$ in (3.6e) has a symmetric spin part and is therefore the triplet with anti-symmetric spatial part, *e.g.* p-wave.

A spin-triplet state is classified as unitary if $\mathrm{i}\boldsymbol{d}_{\boldsymbol{k}} \times \boldsymbol{d}^*_{\boldsymbol{k}} = 0$ and non-unitary otherwise. Furthermore, the average spin of a triplet state is [37]

$$\langle \boldsymbol{S}_{\boldsymbol{k}} \rangle = \mathrm{i}\boldsymbol{d}_{\boldsymbol{k}} \times \boldsymbol{d}^*_{\boldsymbol{k}}, \tag{3.7}$$

which means that only non-unitary triplet states can carry a net magnetic moment.

The spin-triplet pairing can be characterized analogously with that of ^{3}He, where it is divided in two main groups [37]; the A-phase (due to Anderson–Brinkman–Morel) and the B-phase (due to Balian–Werthamer [36]) . The latter has an isotropic energy gap, with $S_z = 0$, *i.e.* $\Delta_{\boldsymbol{k}\uparrow\downarrow} \neq 0$. The A-phase on the other hand, has an anisotropic gap, with

$S_z = \pm 1$. In general, the A-phase has $\Delta_{\boldsymbol{k}\uparrow\downarrow} = 0, \Delta_{\boldsymbol{k}\uparrow\uparrow} \neq 0$, $\Delta_{\boldsymbol{k}\downarrow\downarrow} \neq 0$ and is characterized by *equal spin pairing* (ESP). The A_1-phase has only one gap $\Delta_{\boldsymbol{k}\sigma\sigma} \neq 0$, while $\Delta_{\boldsymbol{k},-\sigma,-\sigma} = 0$. The A_2-phase has $\Delta_{\boldsymbol{k}\uparrow\uparrow} \neq \Delta_{\boldsymbol{k}\downarrow\downarrow} \neq 0$.

Superconducting materials that do not fully conform to the BCS-theory are collectively named *unconventional superconductors*. The original BCS-theory describes s-wave, type-I superconductivity, but it can be generalized to cover other pairing symmetries. In Paper I, II and III [1, 2, 3] we have considered non-unitary triplet pairing which can have a net magnetic moment, as opposed to s-wave where the electrons in the Cooper-pair has opposite spins and thus no magnetic moment.

3.2.4 High-temperature superconductors

As already mentioned, type-II superconductors usually have a much higher critical temperature than type-I superconductors and are therefore often referred to as high-T_c superconductors. As of today, there is no complete microscopic theory for this class of superconductors. Apart from the lack of resistivity in the low-temperature phase, they are fundamentally different from conventional superconductors. Although the superconducting state is due to the formation of Cooper-pairs, the pairing mechanism might be something other than phonon mediated.

One common feature of this group of superconductors is that they contain copper-oxide (CuO_2) layers in the crystal structure. It is believed that it is in this layer that the superconductivity arises. Thus, understanding the physics that is governing this layer—also away from the superconducting state—is of great interest. Paper IV addresses the phase transitions in the high-temperature phase driven by current fluctuations in the two-dimensional layers, see Chapter 5.

3.2.5 Josephson effect

Powered with the BCS-theory, Brian David Josephson was able to investigate what would happen if two superconductors were brought in contact via a weak link, *i.e.* a junction with a critical current much lower than each material on each side. A so-called SIS junction is one example of a weak link, see Figure 2.1 of Section 2.1.1 for a sketch of the setup. His theoretical predictions were published in 1962 [8] and is now known as the Josephson effect. The two main predictions are:

- **DC Josephson effect**. Even when there is no externally applied voltage across the junction, there can be a direct current between the two superconductors that is due to Cooper-pair tunneling. This is the DC Josephson current $I = I_c \sin \Delta\theta$, where $\Delta\theta$ is the superconducting phase difference, and I_c is the critical current.

- **AC Josephson effect**. If a fixed voltage V is applied across the junction, the phase θ will vary linearly with time t and give the frequency $\omega_{\mathrm{J}} \equiv \partial_t(\theta_{\mathrm{R}} - \theta_{\mathrm{L}}) = 2eV/\hbar$. Consequently there will be an AC Josephson current $I = I_{\mathrm{c}} \sin(\Delta\theta + \omega_{\mathrm{J}} t)$.

These predictions are readily observable, and Josephson received the Nobel prize for the discovery in 1973 [38].

For instance, the effect is utilized in SQUIDs (*Superconducting Quantum Interference Devices*), for which various types were invented only a few years after Josephson's prediction. These are instruments based on superconducting loops with Josephson junctions, which makes them extremely sensitive to magnetic fields. In fact, they can be used to measure single flux quanta, and therefore serve as a tool for extremely accurate measurements of any physical quantity that can be converted into a magnetic field. SQUIDs are in commercial use in instruments that measure neural currents in the human brain [28].

3.3 Spin-orbit coupling

When electrons are moving in a magnetic field, they will experience an electric field, and conversely—electrons that move in an electric field will experience a magnetic field. This relativistic interaction between the spin and the motion of electrons is called the *spin-orbit coupling*.

Spin-orbit coupling does not break any symmetries alone, but will reveal itself in non-centrosymmetric crystals (*i.e.* crystals without inversion symmetry), as well as in *e.g.* crystals with impurities, local confinement of electrons or in materials exposed to an external electrical field.

Theoretically, the effect can be derived as a relativistic correction to the Schrödinger equation. If one starts out with the relativistic expression for the kinetic energy of a particle with rest mass m, namely $H^2 = c^2\boldsymbol{p}^2 + m^2c^4$, and then include electric and magnetic potentials, and interpret H and $\boldsymbol{p}$ as operators, one will arrive at a relativistic wave equation for electrons in an electric and magnetic field. This equation can again be cast into the Dirac equation, which upon approximation and comparison with the Schrödinger equation gives the relativistic corrections. One of these is the spin-orbit coupling $\sim (\nabla V \times \boldsymbol{p}) \cdot \hat{\boldsymbol{\sigma}}$.

The electromagnetic potential V can be divided in an *intrinsic* part V_{int} and an *extrinsic* part V_{ext}. The periodic crystal potential is included in V_{int}, whereas V_{ext} is an aperiodic potential due to any impurities, boundaries, or an external electrical field $\boldsymbol{E} = -\nabla V_{\mathrm{ext}}$ [39]. We have focused on the latter, where the Hamiltonian includes a Rashba term $\sim (\boldsymbol{E} \times \boldsymbol{p}) \cdot \hat{\boldsymbol{\sigma}}$, and $\boldsymbol{E}$ is treated as an externally applied electrical field.

Spin-orbit Hamiltonian

The Rasbha spin-orbit Hamiltonian can be written

$$H_{\mathrm{SO}} = \sum_{\boldsymbol{k}} \phi^\dagger_{\boldsymbol{k}} \boldsymbol{B}_{\boldsymbol{k}} \cdot \hat{\boldsymbol{\sigma}} \phi_{\boldsymbol{k}}, \tag{3.8}$$

where $\boldsymbol{B}_{\boldsymbol{k}} = \xi \boldsymbol{E} \times \boldsymbol{k}$, with ξ being a material dependent parameter, and $\boldsymbol{E} = -\nabla V_{\mathrm{ext}}$ is the electrical field felt by the electrons. The basis is $\phi_{\boldsymbol{k}} = (c_{\boldsymbol{k}\uparrow}, c_{\boldsymbol{k}\downarrow})^{\mathrm{T}}$ as in Section 3.1.

3.4 Coexistence

We have now looked at ferromagnetism, superconductivity and spin-orbit coupling as isolated properties, and expressed the respective Hamiltonians in ways that are suitable for being combined. As a closure of this chapter, let us therefore write up the most general Hamiltonian in the current framework. Here, we will simply combine the Hamiltonians mathematically, without going into details on whether this is physically feasible. In the next chapter, however, where Papers I-III are introduced, we shall look at special cases of this.

In order to combine the 2×2 ferromagnetic (3.3) and spin-orbit (3.8) Hamiltonians with the 4×4 superconducting Hamiltonian (3.6b), we need to expand the 2×2 matrices to 4×4 matrices. For this, one can use the general formula

$$\sum_{\boldsymbol{k}} \phi^\dagger_{\boldsymbol{k}} \hat{A}_{\boldsymbol{k}} \phi_{\boldsymbol{k}} = \frac{1}{2} \sum_{\boldsymbol{k}} \varphi^\dagger_{\boldsymbol{k}} \begin{pmatrix} \hat{A}_{\boldsymbol{k}} & 0 \\ 0 & -\hat{A}^{\mathrm{T}}_{-\boldsymbol{k}} \end{pmatrix} \varphi_{\boldsymbol{k}} + \frac{1}{2} \sum_{\boldsymbol{k}} \mathrm{Tr}\, \hat{A}_{\boldsymbol{k}}, \tag{3.9}$$

which is valid for the fermion basis $\varphi_{\boldsymbol{k}} = (\phi_{\boldsymbol{k}}, \phi^{\dagger\mathrm{T}}_{-\boldsymbol{k}})^{\mathrm{T}} = (c_{\boldsymbol{k}\uparrow}, c_{\boldsymbol{k}\downarrow}, c^\dagger_{-\boldsymbol{k}\uparrow}, c^\dagger_{-\boldsymbol{k}\downarrow})^{\mathrm{T}}$. We then arrive at the total Hamiltonian

$$H_{\mathrm{FMSCSO}} = H'_0 - \frac{1}{2} \sum_{\boldsymbol{k}} \varphi^\dagger_{\boldsymbol{k}} \underbrace{\begin{pmatrix} -\hat{A}_{\boldsymbol{k}} & \hat{\Delta}_{\boldsymbol{k}} \\ \hat{\Delta}^\dagger_{\boldsymbol{k}} & \hat{A}^{\mathrm{T}}_{-\boldsymbol{k}} \end{pmatrix}}_{\check{A}_{\boldsymbol{k}}} \varphi_{\boldsymbol{k}} + \frac{1}{2} \sum_{\boldsymbol{k}} \mathrm{Tr}\, \hat{A}_{\boldsymbol{k}}, \tag{3.10}$$

where H'_0 is an irrelevant constant term and $\hat{A}_{\boldsymbol{k}} = \varepsilon_{\boldsymbol{k}} \hat{\sigma}_0 - \boldsymbol{\zeta} \cdot \hat{\boldsymbol{\sigma}} + \boldsymbol{B}_{\boldsymbol{k}} \cdot \hat{\boldsymbol{\sigma}}$, see Eqs. (3.3b), (3.6b) and (3.8).[7]

[7] It is left as an exercise for the reader to show that the energy spectrum of this Hamiltonian is $E = -\lambda/2$, where λ is the solution of the characteristic equation $\det(\check{A}_{\boldsymbol{k}} - \lambda \check{\sigma}_0) = C_4\lambda^4 + C_3\lambda^3 + C_2\lambda^2 + C_1\lambda + C_0 = 0$ in which $C_4 = 1$, $C_3 = 0$ (follows from hermeticity of $\check{A}_{\boldsymbol{k}}$) , $C_2 = -2(\varepsilon^2_{\boldsymbol{k}} + |\boldsymbol{\zeta}|^2 + |\boldsymbol{B}_{\boldsymbol{k}}|^2 + |\boldsymbol{d}_{\boldsymbol{k}}|)$, $C_1 = -8\varepsilon_{\boldsymbol{k}} \boldsymbol{\zeta} \cdot \boldsymbol{B}_{\boldsymbol{k}}$, $C_0 = \varepsilon^4_{\boldsymbol{k}} + |\boldsymbol{\zeta}|^4 + |\boldsymbol{B}_{\boldsymbol{k}}|^4 + \boldsymbol{d}^2_{\boldsymbol{k}}(\boldsymbol{d}^*_{\boldsymbol{k}})^2 + \varepsilon_{\boldsymbol{k}} \boldsymbol{\zeta} \cdot (\mathrm{i}\boldsymbol{d}_{\boldsymbol{k}} \times \boldsymbol{d}^*_{\boldsymbol{k}}) - 2\varepsilon^2_{\boldsymbol{k}}(|\boldsymbol{\zeta}|^2 + |\boldsymbol{d}_{\boldsymbol{k}}|^2 + |\boldsymbol{B}_{\boldsymbol{k}}|^2) - 2(|\boldsymbol{\zeta} \cdot \boldsymbol{d}_{\boldsymbol{k}}|^2 + |\boldsymbol{\zeta} \cdot \boldsymbol{B}_{\boldsymbol{k}}|^2 - |\boldsymbol{B}_{\boldsymbol{k}} \cdot \boldsymbol{d}_{\boldsymbol{k}}|^2) + 2(|\boldsymbol{\zeta} \times \boldsymbol{d}_{\boldsymbol{k}}|^2 + |\boldsymbol{\zeta} \times \boldsymbol{B}_{\boldsymbol{k}}|^2 - |\boldsymbol{B}_{\boldsymbol{k}} \times \boldsymbol{d}_{\boldsymbol{k}}|^2)$.

4 Quantum transport in systems with multiple broken symmetries

In the previous chapter, we looked briefly at Hamiltonians describing ferromagnetism, superconductivity and spin orbit coupling. In this chapter, we will look at combinations of these, and see how they introduce novel effects in quantum transport.

From the discussion in the previous sections it is clear that conventional s-wave superconductivity and isotropic ferromagnetism are mutually excluding properties; the ferromagnetic order will tend to break the opposite spin Cooper-pairs in the superconducting condensate. However, as early as in 1957, Ginzburg[1] proposed that ferromagnetism and superconductivity in fact could coexist [41], although not in the conventional way. Ferromagnetic superconductors have been experimentally confirmed to exist in *e.g.* UGe_2 [42] and in URhGe [43].

Whether the superconducting and ferromagnetic order parameters coexist uniformly, if they are phase separated, or if they only exist as a surface effect, is of course crucial for the understanding. The internal magnetization could in principle lead to an Abrikosov vortex lattice [32, 44], as mentioned in Section 3.2.1. It is, however, possible to avoid this scenario by letting the magnetization stay below the lower critical field H_{c_1} [45].[2]

In order to have true coexisting ferromagnetic and superconducting order intrinsically with bulk order parameters[3], one is most likely to have spin-triplet pairing, where the Cooper-pairs carry a net magnetic moment. Experiments on *e.g.* UGe_2 show [49] that the critical temperature for the superconducting state is higher for larger magnetization. This

[1] Vitaly L. Ginzburg received the Nobel Prize in physics in 2003 for his theoretical work on superconductivity [40].

[2] It is argued quantitatively in Ref. [45] that URhGe is vortex free.

[3] Other choices are also possible, that for instance give rise to helimagnetic/Fulde–Ferrell–Larkin–Ovchinnikov (FFLO/LOFF) order [46, 47, 48].

suggests that ferromagnetism may in fact enhance superconductivity in these compounds. Furthermore, Ref. [50] suggests that the pairing symmetry in URhGe is that of equal spin, indicating p-wave pairing. Ref. [51] argues that the pairing symmetry realized in UGe_2 must be a nonunitary triplet.

When studying transport in such systems, one also needs to consider the orbital effect that may lead to Cooper-pair breakup. This can be avoided by considering thin films with in-plane magnetization.[4]

Why study quantum transport?

The motivation for studying quantum transport in systems with multiple broken symmetries is twofold. First off, it is of great interest to utilize the electron spin degree of freedom—and not only the charge—in electronic devices. Secondly, by measuring for example tunneling currents, one can probe for the symmetry inside materials, *e.g.* the symmetry of the superconducting gap.

When it comes to electron transport in electronic devices, in most cases, only the electron charge current is utilized, where for example the binary numbers 0 and 1 are represented by "no current" and "current". Notable exceptions to this is the GMR (Giant Magneto Resistance), in which the electron spin plays a central role in the reading head of almost all conventional hard drives nowadays. GMR was discovered independently by Albert Fert and Peter Grünberg [53, 54], and they received the Nobel prize in physics in 2007 for their discovery [55].

Ideally, one would like to utilize both the charge and spin degree of freedom of the electron, in order to produce *e.g.* a spin-current without a charge-current etc. One aim is to create smaller and more energy efficient devices, but one is also interested in more sophisticated effects such as entanglement and quantum computing, where quantum mechanical nature of the electron is more prominent.

Moreover, studying systems with simultaneous broken symmetries offers a plethora of new physics and therefore possibly yet unforeseen effects which can lead to new applications. Since these systems are so rich in physics, they give us the opportunity to learn if the tunneling currents can be controlled by means of external control parameters. This is of course of great interest when it comes to inventing new electronic devices.

So quantum transport plays an important role in nanotechnology, spintronics and information and communication technology (ICT) in general, but it also important for understanding the fundamental underlying physics in unconventional materials.

In the next sections, the three first papers will be introduced.

[4] Ginzburg actually suggests thin films in his Nobel lecture [52] with references to his paper [41].

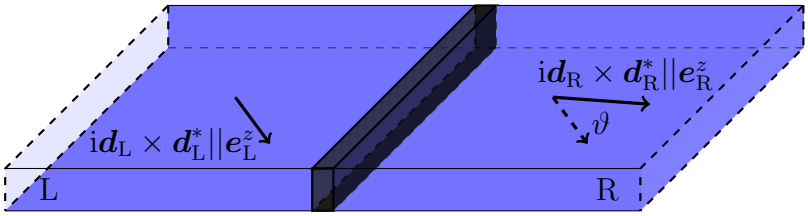

Figure 4.1: Tunneling of Cooper-pairs between two thin-film non-unitary ferromagnetic superconductors with non-collinear magnetization.

4.1 Josephson effect in ferromagnetic superconductors

In Paper I [1] we present a model describing tunneling between two ferromagnetic superconductors and give the resulting charge- and spin-currents. Paper II [2] is a follow-up on the first, where about one half is devoted to a more detailed discussion on this (the second part is discussed in the Section 4.2).

Figure 4.1 shows two thin film non-unitary ferromagnetic superconductors with spin-triplet p-wave pairing symmetry. They are connected via a thin insulating layer that is assumed to be spin-inactive. We have studied the Josephson effect that arises in such a setup. As mentioned in Section 3.2.3, the non-unitary state means that the Cooper-pairs can carry a net magnetic moment, and can therefore be compatible with bulk ferromagnetic order.

It is assumed that the strength of the internal magnetization is weak enough to avoid formation of an Abrikosov flux-lattice, and the reason for studying thin films is to make sure that the orbital effect does not break the Cooper-pairs. The ferromagnetic and superconducting order parameters are assumed to coexist uniformly, and the superconductor is in general assumed to be in the A_2-phase, with[5] $\Delta_{\boldsymbol{k}\uparrow\uparrow} \neq \Delta_{\boldsymbol{k}\downarrow\downarrow} \neq 0$ and $\Delta_{\boldsymbol{k}\uparrow\downarrow} = 0$ (see Section 3.2.3).

The ferromagnetic superconductors can be thought to have arisen out of a ferromagnetic state, where the same itinerant electrons that give rise to ferromagnetism condense into Cooper-pairs.

Our starting point is the spin generalized number operator $N_{\alpha\beta} = \sum_{\boldsymbol{k}} c^\dagger_{\boldsymbol{k}\alpha} c_{\boldsymbol{k}\beta}$, for which we calculate the time evolution by expressing it in the interaction picture, and find the general spin- and charge-currents by using the Kubo formula. Following the details given in Paper I and II [1, 2], we arrive at the resulting, general spin- and charge-current between the two

[5] An A_1-phase can be considered as a special case by letting $\Delta_{\boldsymbol{k}\sigma\sigma} = 0$ while $\Delta_{\boldsymbol{k},-\sigma,-\sigma} \neq 0$.

sides, for zero bias voltage, namely

$$I_{\mathrm{J},z}^{\binom{\mathrm{C}}{\mathrm{S}}} = \sum_{\boldsymbol{kp}\alpha\beta} \begin{pmatrix} -e \\ \alpha \end{pmatrix} |T_{\boldsymbol{kp}}|^2 \left[1 + \alpha\beta\cos(\vartheta)\right] \sin(\theta^{\mathrm{L}}_{\beta\beta} - \theta^{\mathrm{R}}_{\alpha\alpha}) \times \frac{|\Delta_{\boldsymbol{k}\alpha\alpha}||\Delta_{\boldsymbol{p}\beta\beta}|}{E_{\boldsymbol{k}\alpha}E_{\boldsymbol{p}\beta}} \cos(\theta_{\boldsymbol{p}} - \theta_{\boldsymbol{k}}) F_{\boldsymbol{kp}\alpha\beta} \tag{4.1a}$$

where

$$F_{\boldsymbol{kp}\alpha\beta} = -\frac{1}{2}\sum_{\pm} \frac{f(\pm E_{\boldsymbol{k}\alpha}) - f(E_{\boldsymbol{p}\beta})}{E_{\boldsymbol{k}\alpha} \mp E_{\boldsymbol{p}\beta}}. \tag{4.1b}$$

Here I_{J}^{C} is the charge Josephson current, and $I_{\mathrm{J},z}^{S}$ is the z component of the spin Josephson current. Note that the equation is written in a condensed way, such that the $\boldsymbol{k}$ and $\boldsymbol{p}$ indices implicitly mean the right and left side of the junction, respectively. $E_{\boldsymbol{k}\alpha} = \sqrt{\xi^2_{\boldsymbol{k}\alpha} + |\Delta_{\boldsymbol{k}\alpha\alpha}|^2}$; $\xi_{\boldsymbol{k}\alpha} = \varepsilon_{\boldsymbol{k}\alpha} - \mu_{\mathrm{R}}$; $\varepsilon_{\boldsymbol{k}\alpha} = \varepsilon_{\boldsymbol{k}} - \alpha\zeta^{\mathrm{R}}_z$, and similarly for the left side with $\mathrm{R} \to \mathrm{L}$ and $\boldsymbol{k} \to \boldsymbol{p}$. The spin indices are $\alpha, \beta \in \pm 1$. Also note that Eq. (4.1a) can be written as $I = I_0 + I_{\mathrm{m}}\cos(\vartheta)$. This means that the critical Josephson current can be controlled by the twist in the magnetization across the junction.

Note that the definition of the spin current we have used is *the rate at which the spin vector* $\boldsymbol{S}$ *on one side of the junction changes as a result of tunneling across the junction* [1].

4.2 Tunneling currents in ferromagnets with spin-orbit coupling

In Paper II [2] we investigate how ferromagnetism and spin-orbit coupling affect the tunneling currents. Our approach is to calculate the general result for the spin and charge currents between two ferromagnets with spin-orbit coupling, and then consider important geometries and physical limits.

Figure 4.2 shows a general tunneling junction consisting of two ferromagnets with spin-orbit coupling separated by an insulating tunneling barrier.

Starting from a general Heisenberg ferromagnet in three dimensions, we add a Rashba spin-orbit term in order to describe a quite general system. We are then able to express the Hamiltonian by a 2×2 matrix which is the sum of (3.3) and (3.8) in addition to the free Fermi gas term $\sum_{\boldsymbol{k}\sigma} \varepsilon_{\boldsymbol{k}} c^{\dagger}_{\boldsymbol{k}\sigma} c_{\boldsymbol{k}\sigma}$.

Upon calculating the time evolution of the spin generalized number operator, by utilizing the Kubo formula (2.16), the Matsubara–Green formalism (see Section 2.2), we find the z-component of the (one particle) spin current for zero bias voltage (Eq. (53) in Paper

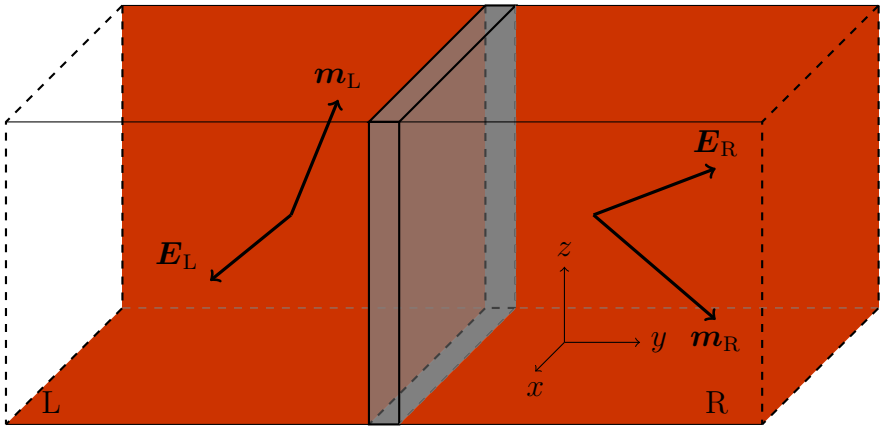

Figure 4.2: Two ferromagnetic metals with spin-orbit coupling separated by a thin insulating barrier. The magnetization $\boldsymbol{m}$ and electrical field $\boldsymbol{E}$ are allowed to point in any direction so that the results are generally valid, while special cases such as planar magnetization etc. are easily obtained by applying the proper limits to the general expressions.

II [2]). The charge current is naturally zero in this case. Special cases, such as specific geometries, are discussed.

The main result is that, in the general case where both ferromagnetism and spin-orbit coupling are included, there is an additional term in the spin-current that describes an interplay between the spin-orbit interaction and the ferromagnetic order. In the spin channel we have therefore found a term that is more than just the sum of the individual contributions.

4.3 Conductance spectra

In Paper III [3] we look at the conductance spectra in a junction consisting of a ferromagnetic metal and a non-unitary ferromagnetic superconductor. We predict that the conductance spectra will provide detailed information about the pairing symmetry of the superconductor.

As mentioned before, finding ways of getting information about the symmetry of the superconducting phase is important to understand unconventional superconductivity.

In contrast to Paper I and II, where we studied tunneling currents by using the tunneling formalism (see Section 2.1.1), we here utilize a spin generalized BTK formalism (see Section 2.3) to account for surface effects and to allow for varying barrier strengths. Although one in general would expect the proximity effect at the surface to cause the superconducting gap to leak into the ferromagnetic region, we have disregarded this effect and modeled the gap as a step function at the interface. Since we have one ferromagnet in the superconducting

state and one ferromagnet in the normal state, there will be no Josephson current in the problem.

In accordance with the discussion in the preceding sections, we have studied a thin film of a ferromagnetic superconductor in a non-unitary spin-triplet state with equal spin-pairing, *i.e.* an A_2-phase equivalent (see Section 3.2.3).

Our starting point is the Bogoliubov-de Gennes (BdG) equation for the ferromagnetic superconductor, which is nothing but the eigenvector equation for the transformation matrix which diagonalize the Hamiltonian—in this case $\check{A}_{\boldsymbol{k}}$ given in Eq. (3.10) with $\boldsymbol{B}_{\boldsymbol{k}} = 0$.[6] The spin-dependent coherence factors of these eigenvectors are then the wave-function solutions that turn up in the reflection coefficients, which let us calculate the conductance.

We show how the conductance spectra provide information about the superconducting gaps, specifically the magnitude of the various components of the gap, and possibly their relative orientation in $\boldsymbol{k}$-space. The latter can be seen due to the formation of zero bias conductance peaks for certain pairing-symmetries.

[6] In Paper III a slightly different sign-convention is used, in accordance with [56].

5 High-T_c cuprates

In Paper IV [4], we have studied a model describing thermal orbital current-fluctuations in the CuO_2 layers of high-T_c superconducting cuprates in the non-superconducting state. This was done by large scale Monte Carlo simulations. A microscopic theory supporting ordering of such currents was first proposed by Chandra Varma [57]. Details on the derivation of the effective theory can be found elsewhere [58, 59].

We have considered the classical part of the effective Hamiltonian, which is described by two intrinsically anisotropic Ising models, coupled by an Ashkin–Teller four-spin term [60, 61, 62], as well as a next-nearest neighbor term favoring striped order. The effective Hamiltonian reads

$$H = -\sum_{\langle i,j\rangle} \left(K_{ij}^x \sigma_i \sigma_j + K_{ij}^y \tau_i \tau_j\right) - \sum_{\langle\langle i,j\rangle\rangle} K_{ij}^{xy} (\tau_i \sigma_j + \sigma_i \tau_j) - K_4 \sum_{\langle i,j\rangle} \sigma_i \sigma_j \tau_i \tau_j, \tag{5.1}$$

where $\sigma_i, \tau_i \in \pm 1$ are Ising variables representing the coherent part of the orbital current in the x- and y-directions through the Cu-sites, respectively, see Figure 5.1. In the sums $\langle \cdot, \cdot \rangle$ and $\langle\langle \cdot, \cdot \rangle\rangle$ denotes nearest and next-nearest neighbors, respectively.

The two Ising parts are both intrinsically anisotropic, where the anisotropy is of equal strength but in opposite direction. More precisely we have the anisotropy parameter $A \equiv K_t/K_l$ and

$$K_{ij}^x = \begin{cases} K_l & \text{for } j = i \pm \hat{x} \\ K_t & \text{for } j = i \pm \hat{y} \end{cases} \qquad K_{ij}^y = \begin{cases} K_t & \text{for } j = i \pm \hat{x} \\ K_l & \text{for } j = i \pm \hat{y} \end{cases}, \tag{5.2}$$

where $K_l, K_t > 0$ and $\hat{x}$ and $\hat{y}$ represent the lattice constant in the x- and y-directions, respectively. The critical temperature for the ordered phase, in the case where $K_{ij}^{xy} = K_4 = 0$ and $A = 1$, is therefore at the Ising critical temperature, $T_c \simeq 2.269$.

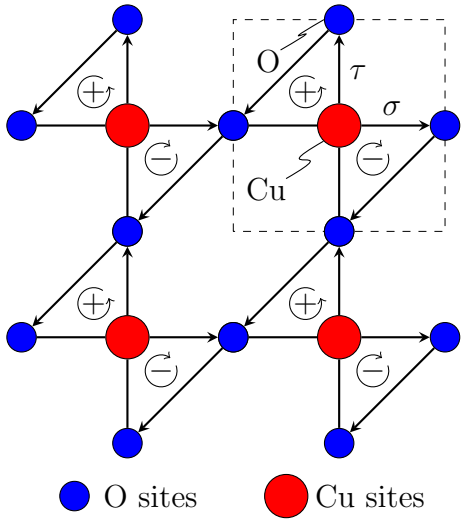

Figure 5.1: An ordered current pattern in a CuO_2 plane.

The K_{ij}^{xy} coupling term is of opposite sign in the two diagonal directions;

$$K_{ij}^{xy} = \begin{cases} K_3 & \text{for } j = i \pm (\hat{x} + \hat{y}) \\ -K_3 & \text{for } j = i \pm (\hat{x} - \hat{y}) \end{cases} \tag{5.3}$$

with $K_3 > 0$. In (5.1), K_4 is constant and will take *negative values*, $K_4 < 0$, favoring anti-ferromagnetic ordering of the composite spins $\sigma_i \tau_i$.

The phase diagram for high-T_c superconducting cuprates is given in Figure 5.2. Inspired by experiments [63, 64], we have studied the phase transition from ordered to disordered orbital currents, which corresponds to the pseudogap to strange metal transition in the figure. This in order to see if the model features a lack of specific heat anomaly across this line, while at the same time exhibit an anomaly in the susceptibility of the staggered magnetization. This staggered magnetization, which is a measure of the ordering of the orbital currents, is given by

$$M_{\text{so}} \equiv \sqrt{\frac{\langle \boldsymbol{m} \rangle^2}{2}} = \sqrt{\frac{\langle m^x \rangle^2 + \langle m^y \rangle^2}{2}}, \tag{5.4}$$

where $\boldsymbol{m} = \boldsymbol{S} \equiv (m^x, m^y)$, $m^x = \sum_i \sigma_i$ and $m^y = \sum_i \tau_i$. Since this order parameter is not directly measurable, and since the breakup of this ordering does not lead to a specific heat anomaly, this is often referred to as *hidden order*.

We show that in a limited parameter regime, the model exhibit a substantially suppressed specific heat anomaly at the transition from disordered to ordered orbital currents.

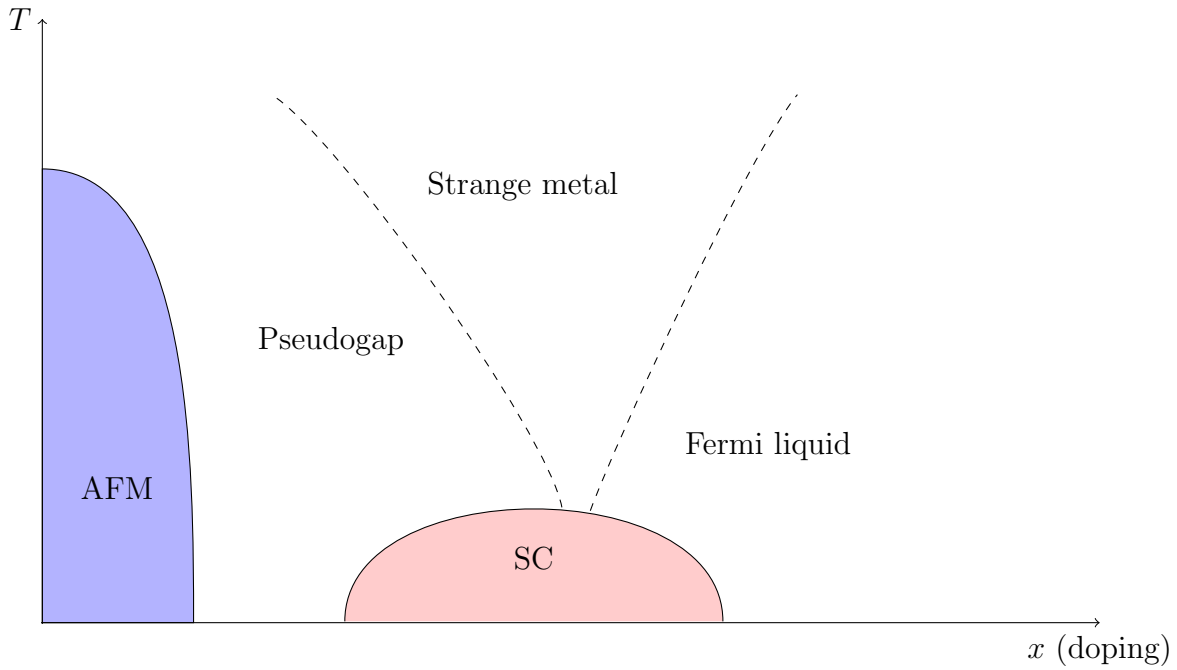

Figure 5.2: Temperature (T) vs. doping (x) phase diagram for high-T_c superconductivity. For low doping we have an anti-ferromagnetic phase (AFM), and for intermediate doping and low temperature we have a superconducting phase (SC).

6 Acknowledgments

What is it like to do a PhD?

> Imagine yourself in a plane high up in the sky on a sunny day. Then jump out—without a parachute. This is the beginning of your PhD study, characterized by **uncertainty**, **excitement** and a lot of **freedom**.
>
> *What do you see?* First off, you get a very **nice view** and you get to study some areas in great detail from a whole **new angle**. Your supervisor gives you a set of tools you need to put together your parachute.
>
> After some time, you break the cloud layer. It gets a bit rainy now and then, and you **might panic** a little bit. But in the end, you have published a few papers, and you are able to write a thesis that patch them all together to form your little parachute that hopefully will **save your skin**.
>
> At this point you are finally able to really **understand** some of the details, but now you don't have the **time** to study them before you have to pull the cord.
>
> New challenges await.

I would first like to express my utmost gratitude to my supervisor Professor Asle Sudbø. In our search for novel physics in fields where "no man has gone before", I have been fumbling with the map, blinded by the details, trying to calculate where we are, while Asle has been gazing at the horizon, already pretty certain about the direction to go, and even what we would find. Your endless enthusiasm is honorable. When all I could see was trouble and despair, all of the sudden you would spot something interesting right "out of nowhere". Sometimes, this has been stuff that eventually got published in a journal. When I felt that I was stuck in yet another dead end, having calculated something that turned out to be zero etc., you have pointed out a new direction which has lead somewhere.

I'm also grateful to Professors Flavio Nogueria, James F. Annett and Arne Brataas for serving as my evaluation committee for this thesis, as well as the defense 30. May 2008.

There are a lot of people I would like to thank for making my everyday life into a pleasant

experience, both at work and elsewhere. Jan Petter Morten and I have followed the same education since high school and all the way through our PhD studies. I have enjoyed every part of it! I also appreciate the unstructured happiness experienced while living together with Endre Berntsen Håland—you have tought me a lot of stuff well worth knowing.

I have really appreciated the extremely nice atmosphere among the Post Docs and PhD students at the department of physics, where we can discuss everything from hardcore physics to everyday trivialities in our coffee-breaks, and whenever else. This is one of the things I certainly will miss a lot, in addition to the many off-campus activities we have enjoyed. In particular, I would like to thank (possibly in quasi-chronological order): Jan Øystein Haavik Bakke, Kjetil Børkje, Christian Andre Andresen, Lars Erik Walle, Thomas Ramstad, Jo Smiseth, Stein Olav Skrøvseth, Eivind Smørgrav, Per Kristian Hove, Øyvind Krøvel-Velle Standal, Håvard Norum, Trygve Kristiansen, Steinar Kragset, Eskil Kulseth Dahl, Frantz Stabo-Eeg, Jan Manschot, Kjersti Morten, Terje Røsten, Anh Kiet Nguyen, Egor Babaev, Daniel Huertas-Hernando, Dionne C. G. Klein, Bjarte Gees Bokn Solheim Jon-Mattis Børven, Joakim Hove, Jacob Linder, Mathieu Taillefumier, and Trond Bergh Nilssen.

I also thank Jacob and Mathieu for careful proofreading of the introductory part of this thesis and for giving valuable feedback that has helped improving the text.

The NordForsk Nordic network of low-dimensional physics is acknowledged for hosting many meetings where I and others have had the opportunity to widen our physical understanding in various fields.

My whole family has always been there for me. My mom Nina, my dad Bent, Christine, Ingrid, Olav, Hans Henrik, and all of my extended family; I thank you all!

Finally, I thank my beloved Edrun Andrea and daughter Maren. You mean everything to me!

Martin S. Grønsleth

Bibliography

[1] M. S. Grønsleth, J. Linder, J.-M. Børven, and A. Sudbø, Physical Review Letters **97**, 147002 (2006), doi:10.1103/PhysRevLett.97.147002, [link].

[2] J. Linder, M. S. Grønsleth, and A. Sudbø, Physical Review B **75**, 024508 (2007), doi:10.1103/PhysRevB.75.024508, [link].

[3] J. Linder, M. S. Grønsleth, and A. Sudbø, Physical Review B **75**, 054518 (2007), doi:10.1103/PhysRevB.75.054518, [link].

[4] M. S. Grønsleth, E. K. Dahl, T. B. Nilssen, C. M. Varma, and A. Sudbø, Specific heat, order parameter, and magnetic susceptibility from fluctuating orbital currents in high-T_c superconducting cuprates, preprint, 2008.

[5] E. K. U. Gross, E. Runge, and O. Heinonen, *Many-Particle Theory*, Adam Hilger, 1991.

[6] F. Mandl and G. Shaw, *Quantum Field Theory*, Wiley, 1993.

[7] M. H. Cohen, L. M. Falicov, and J. C. Phillips, Phys. Rev. Lett. **8**, 316 (1962), doi:10.1103/PhysRevLett.8.316, [link].

[8] B. D. Josephson, Physics Letters **1**, 251 (1962), [link].

[9] R. E. Prange, Phys. Rev. **131**, 1083 (1963), doi:10.1103/PhysRev.131.1083, [link].

[10] T. Matsubara, Prog. Theor. Phys **14**, 351 (1955).

[11] G. D. Mahan, *Many-Particle Physics*, Kluwer Academic/Plenum Publishers, 3. edition, 2002.

[12] A. M. Zagoskin, *Quantum Theory of Many-Body Systems: Techniques and Applications*, Springer, 1998.

[13] R. Kubo, J. Phys. Soc. Jpn. **12**, 570 (1957), doi:10.1143/JPSJ.12.570, [link].

[14] R. Kubo, M. Yokota, and S. Nakajima, J. Phys. Soc. Jpn. **12**, 1203 (1957), doi:10.1143/JPSJ.12.1203, [link].

[15] G. E. Blonder, M. Tinkham, and T. M. Klapwijk, Phys. Rev. B **25**, 4515 (1982), doi:10.1103/PhysRevB.25.4515, [link].

[16] E. H. Hauge, Go critical!, Lecture notes, NTNU, 2001.

[17] E. Ising, Z. Phys. **31**, 253 (1925), doi:10.1002/andp.19414320403.

[18] L. Onsager, Phys. Rev. **65**, 117 (1944), doi:10.1103/PhysRev.65.117.

[19] N. Metropolis, A. W. Rosenbluth, M. N. Rosenbluth, A. H. Teller, and E. Teller, J. Chem. Phys. **21**, 1087 (1953), doi:10.1063/1.1699114, [link].

[20] W. K. Hastings, Biometrika **57**, 97 (1970).

[21] R. H. Swendsen and J.-S. Wang, Phys. Rev. Lett. **58**, 86 (1987), doi:10.1103/PhysRevLett.58.86, [link].

[22] M. S. S. Challa, D. P. Landau, and K. Binder, Phys. Rev. B **34**, 1841 (1986), doi:10.1103/PhysRevB.34.1841, [link].

[23] K. Binder, editor, *The Monte Carlo method in condensed matter physics*, volume 71 of *Topics in Applied Physics*, Springer, 1992.

[24] D. P. Landau, Phys. Rev. B **13**, 2997 (1976), doi:10.1103/PhysRevB.13.2997, [link].

[25] D. P. Landau and K. Binder, *A guide to monte carlo simulations in statistical physics*, Cambridge University Press, Cambridge, 2000.

[26] H. K. Onnes, Leiden Comm. **120b, 122b, 124c** (1911).

[27] W. Meissner and R. Ochsenfeld, Naturwissenschaften **21**, 787 (1933).

[28] K. Fossheim and A. Sudbø, *Superconductivity: Physics and Applications*, John Wiley & Sons, London, 2004, doi:10.1002/0470020784.fmatter.

[29] G. Bednorz and K. A. Müller, Z. Phys. B **64** (1986), [link].

[30] M. K. Wu et al., Phys. Rev. Lett. **58**, 908 (1987), doi:10.1103/PhysRevLett.58.908, [link].

[31] The Nobel Prize in Physics, 1987, J. Georg Bednorz and K. Alexander Müller: "for their important break-through in the discovery of superconductivity in ceramic materials".

[32] A. A. Abrikosov, Zh. Eksp. Teor. Fiz. **32**, 1442 (1957).

[33] J. Bardeen, L. N. Cooper, and J. R. Schrieffer, Phys. Rev. **108**, 1175 (1957), doi:10.1103/PhysRev.108.1175, [link].

[34] L. N. Cooper, Phys. Rev. **104**, 1189 (1956), doi:10.1103/PhysRev.104.1189, [link].

[35] The Nobel Prize in Physics, 1972, John Bardeen, Leon Neil Cooper and John Robert Schrieffer: "for their jointly developed theory of superconductivity, usually called the BCS-theory".

[36] R. Balian and N. R. Werthamer, Phys. Rev. **131**, 1553 (1963), doi:10.1103/PhysRev.131.1553, [link].

[37] A. J. Leggett, Rev. Mod. Phys. **47**, 331 (1975), doi:10.1103/RevModPhys.47.331, [link].

[38] The Nobel Prize in Physics, 1973, Brian David Josephson: "for his theoretical predictions of the properties of a supercurrent through a tunnel barrier, in particular those phenomena which are generally known as the Josephson effects", Leo Esaki and Ivar Giaever: "for their experimental discoveries regarding tunneling phenomena in semiconductors and superconductors, respectively".

[39] H.-A. Engel, E. I. Rashba, and B. I. Halperin, Theory of spin hall effects, 2006, Theory of Spin Hall Effects in Semiconductors, in Handbook of Magnetism and Advanced Magnetic Materials, H. Kronmüller and S. Parkin (eds.). John Wiley & Sons Ltd, Chichester, UK, pp 2858-2877 (2007).

[40] The Nobel Prize in Physics, 2003, Alexei A. Abrikosov, Vitaly L. Ginzburg and Anthony J. Leggett: "for pioneering contributions to the theory of superconductors and superfluids".

[41] V. L. Ginzburg, Sov. Phys. JETP **4**, 153 (1957).

[42] S. S. Saxena et al., Nature **406**, 587 (2000), [link].

[43] D. Aoki et al., Nature **413**, 613 (2001), [link].

[44] S. Tewari, D. Belitz, T. R. Kirkpatrick, and J. Toner, Phys. Rev. Lett. **93**, 177002 (2004), [link].

[45] V. P. Mineev, Comptes Rendus Physique **7**, 35 (2006), doi:doi:10.1016/j.crhy.2005.11.006.

[46] P. Fulde and R. A. Ferrell, Phys. Rev. **135**, A550 (1964), doi:10.1103/PhysRev.135.A550, [link].

[47] A. I. Larkin and Y. N. Ovchinnikov, Zh. Exp. Teor. Fiz. **47**, 1136 (1964), [Sov. Phys. JETP 20, 762 (1965)].

[48] I. Eremin, F. S. Nogueira, and R.-J. Tarento, Phys. Rev. B **73**, 054507 (2006), doi:10.1103/PhysRevB.73.054507, [link].

[49] A. Huxley et al., Phys. Rev. B **63**, 144519 (2001), doi:10.1103/PhysRevB.63.144519.

[50] F. Hardy and A. D. Huxley, Phys. Rev. Lett. **94**, 247006 (2005), doi:10.1103/PhysRevLett.94.247006, [link].

[51] K. Machida and T. Ohmi, Phys. Rev. Lett. **86**, 850 (2001), doi:10.1103/PhysRevLett.86.850, [link].

[52] V. L. Ginzburg, Rev. Mod. Phys. **76**, 981 (2004), doi:10.1103/RevModPhys.76.981, [link].

[53] M. N. Baibich et al., Phys. Rev. Lett. **61**, 2472 (1988), doi:10.1103/PhysRevLett.61.2472.

[54] G. Binasch, P. Grünberg, F. Saurenbach, and W. Zinn, Phys. Rev. B **39**, 4828 (1989), doi:10.1103/PhysRevB.39.4828.

[55] The Nobel Prize in Physics, 2007, Albert Fert and Peter Grünberg: "for the discovery of Giant Magnetoresistance".

[56] B. J. Powell, J. F. Annett, and B. L. Györffy, Journal of Physics A **36**, 9289 (2003), [link].

[57] C. M. Varma, Physical Review B (Condensed Matter and Materials Physics) **73**, 155113 (2006), doi:10.1103/PhysRevB.73.155113, [link].

[58] K. Børkje, *Theoretical Studies of Unconventional Order in Quantum Many-Particle Systems*, PhD thesis, NTNU, 2008.

[59] K. Børkje and A. Sudbø, Effective theory of fluctuating circulating currents in high-tc cuprates, preprint.

[60] J. Ashkin and E. Teller, Phys. Rev. **64**, 178 (1943), doi:10.1103/PhysRev.64.178, [link].

[61] C. Fan, Physics Letters A **39**, 136 (1972), doi:doi:10.1016/0375-9601(72)91051-1, [link].

[62] R. J. Baxter, *Exactly Solved Models in Statistical Mechanics*, Academic Press, 1982.

[63] B. Fauqué et al., Physical Review Letters **96**, 197001 (2006), doi:10.1103/PhysRevLett.96.197001, [link].

[64] H. A. Mook, Y. Sidis, B. Fauque, V. Baledent, and P. Bourges, Observation of magnetic order in a $YBa_2Cu_3O_{6.6}$ superconductor, 2008.

Index

Paper I

Interplay between Ferromagnetism and Superconductivity
in Tunneling Currents
Physical Review Letters, 97, 147002 (2006)

Paper II

Tunneling currents in ferromagnetic systems
with multiple broken symmetries
Physical Review B, 75, 024508 (2007)

Is not included due to copyright

Paper III

Conductance spectra of ferromagnetic superconductors: Quantum transport in a ferromagnetic metal/non-unitary ferromagnetic superconductor junction
Physical Review B, 75, 054518 (2007)

Paper IV

Specific heat, order parameter, and magnetic susceptibility from fluctuating orbital currents in high-T_c superconducting cuprates

Preprint

Specific heat, order parameter, and magnetic susceptibility from fluctuating orbital currents in high-T_c superconducting cuprates

M. S. Grønsleth,[1] T. B. Nilssen,[1] E. K. Dahl,[1] C. M. Varma,[2] and A. Sudbø[1]

[1] *Department of Physics, Norwegian University of Science and Technology, N-7491 Trondheim, Norway*
[2] *Department of Physics and Astronomy, University of California, Riverside, CA 92521, USA*

(Dated: Received March 28, 2008)

We have performed large-scale Monte Carlo simulations on a two-dimensional generalised Ising model of thermally fluctuating orbital currents in CuO_2-plaquettes of high-T_c cuprates. The Ising variables represent $Cu-Cu$ bond-currents on the lattice. The model features intrinsically anisotropic Ising couplings, as well as an anisotropic next-nearest neighbor interaction which tends to frustrate uniform ordering in the system. In addition, the model features an Ashkin–Teller nearest-neighbor four-spin coupling. We find that the specific heat features a substantially suppressed anomaly compared to the logarithmic singularity of the $2D$ Ising model. The anomaly does not appear to scale with system size for finite antiferromagnetic Ashkin–Teller coupling. We also compute the staggered magnetization of the system associated with ordering of the orbital currents. We find that the staggered magnetization as well as its susceptibility has the same characteristics as for the $2D$ Ising model with a pronounced and easily discernible non-analytic behavior across the order-disorder transition. The non-analytic behavior of the staggered magnetization implies that a field-induced *uniform* magnetisation also will feature non-analyticities across the phase transition. A prediction from our calculations is therefore that a uniform field-induced magnetization M_0 should have a non-analytic behavior across the pseudogap line of high-T_c cuprates on the underdoped side, as the staggered orbital magnetic moment originating with the orbital currents within each unit cell sets in. Specifically, we predict that M_0 induced by a magnetic field H perpendicular to the CuO_2-plane will have the form $H/M_0 = A + B\ \Theta(T_c - T)\ |1 - T/T_c|^{2\beta}$, where Θ is a step-function, and β is a non-universal order-parameter exponent of the *staggered* magnetisation with a value $1/8 < \beta < 1/4$.

PACS numbers: 74.20.Rp, 74.50.+r, 74.20.-z

I. INTRODUCTION

It has recently been proposed that quantum critical fluctuations associated with the breakup of a particular form of hidden order in high-T_c cuprate superconductors could be responsible for the anomalous transport properties of these compounds[1], by producing a Marginal Fermi Liquid[2]. Within this scenario, these fluctuations would also provide a $d_{x^2-y^2}$ pairing glue in the normal state[1]. The particular form of proposed hidden order involves circulating currents within a CuO_2 unit cell where the currents run horizontally and vertically through a Cu site and close by direct hopping between O orbitals. This results in a pattern of *staggered* orbital magnetic moments within each CuO_2 unit cell, in such a way that the magnetic pattern repeats from unit cell to unit cell, as depicted in Fig. 1. (See also Fig. 1 of Refs. 1,3). These circulating current patterns are generated by a nearest-neighbor repulsion V between Cu and O-atoms in the CuO_2-sheets. The effect of such a repulsive V-term has been extensively investigated in $1D$ CuO-chains, where it has been shown to drive charge-transfer instabilities and superconductivity[5–7]. Other types of current-patterns and charge-fluctuations are also possible[8,9]. The circulating-current pattern does not alter the translational symmetry of the underlying CuO_2-lattice. Significantly, it does not lead to a doubling of the unit cell, in contrast to what is the case for d-density waves[10].

We note that there now seems to be substantial experimental evidence[11,12] in favor of the current-pattern proposed in Fig. 1. It is therefore important to investigate whether or not the proposed models for these novel broken symmetries would predict the lack or presence of prominent signals in such quantities as specific heat or (indirectly) magnetisation. While the current pattern shown in Fig. 1 provides a staggered magnetisation and no net magnetism in the system, it is well known that an antiferromagnetic-to-paramagnetic phase-transition will show up as non-analyticities in the uniform magnetic susceptibility as well. Measuring the uniform magnetic susceptibility is relatively straightforward. In the context of the phasediagram of the cuprates, we want to investigate the possibility of breaking up an Ising-like order associated with staggered circulating currents within a CuO_2 unit cell, without having an observable logarithmic singularity in the specific heat, while at the same time having observable non-analyticities as a function of temperature in a field-induced uniform magnetisation.

The effective model we will perform Monte Carlo simulations on, has been derived elsewhere[3,4]. The action S is written on the form $S = S_{\rm C} + S_{\rm Q}$, where $S_{\rm C}$ is the classical piece of the action, and $S_{\rm Q}$ is part of the action that is needed in the quantum domain of the theory. In this paper, we will focus on discussing the effects of thermal fluctuations, and will there not need $S_{\rm Q}$. The classical

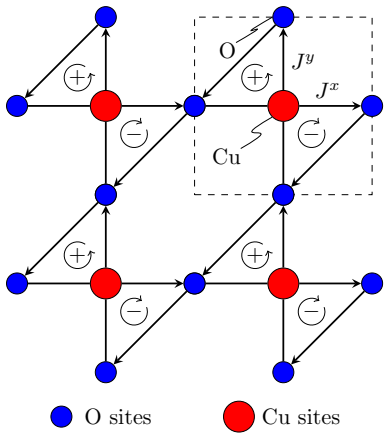

FIG. 1: (Color online) The circulating current phase Θ_{II}[1]. The Cu sites are red circles, O sites are blue. The unit cell is shown by the dashed square. A staggered magnetic moment pattern within each unit cell that repeats from unit cell to unit cell (the curl of the directed circles) is indicated. The currents J^x and J^y represent the horizontal end vertical currents, respectively, to be used in the derived effective model, Eqs. 1 and 2 below. Physically, they represent the *coherent parts* of the orbital fermionic currents in the problem.

piece of the action, $S_{\rm C}$, is given by[3,4]

$$S_{\rm C} = - \beta \sum_{\langle \mathbf{r},\mathbf{r}'\rangle} (K_x \; J^x_{\mathbf{r}} J^x_{\mathbf{r}'} + K_y \; J^y_{\mathbf{r}} J^y_{\mathbf{r}'}) - \beta \sum_{\langle\langle \mathbf{r},\mathbf{r}'\rangle\rangle} K^{xy} \left(J^x_{\mathbf{r}} J^y_{\mathbf{r}'} + J^y_{\mathbf{r}} J^x_{\mathbf{r}'} \right). \quad (1)$$

Here, $\langle \mathbf{r},\mathbf{r}'\rangle$ and $\langle\langle \mathbf{r},\mathbf{r}'\rangle\rangle$ denote nearest-neighbor and next-nearest-neighbor summations, respectively. For $\mathbf{r}-\mathbf{r}' = \pm\hat{\mathbf{x}}$, $K_x = K_l$ and $K_y = K_t$, whereas when $\mathbf{r}-\mathbf{r}' = \pm\hat{\mathbf{y}}$, $K_x = K_t$ and $K_y = K_l$. The parameter $K^{xy} = K_3$ when $\mathbf{r}-\mathbf{r}' = \pm(\hat{\mathbf{x}}+\hat{\mathbf{y}})$ and $K^{xy} = -K_3$ when $\mathbf{r}-\mathbf{r}' = \pm(\hat{\mathbf{x}}-\hat{\mathbf{y}})$. Finally, $\beta = 1/T$ where T is temperature, and we work in units where Boltzmann's constant $k_B = 1$. We will in the following also need the anisotropy parameter $A \equiv K_t/K_l$. Fluctuations ($J^x_{\mathbf{r}} \to -J^x_{\mathbf{r}}, J^y_{\mathbf{r}} \to J^y_{\mathbf{r}}$) corresponds to going from the depicted current pattern (Fig. 1) to a new one which is obtained by a counterclockwise rotation by $\pi/2$, ($J^x_{\mathbf{r}} \to J^x_{\mathbf{r}}, J^y_{\mathbf{r}} \to -J^y_{\mathbf{r}}$) corresponds to clockwise rotation of $\pi/2$, and ($J^x_{\mathbf{r}} \to -J^x_{\mathbf{r}}, J^y_{\mathbf{r}} \to -J^y_{\mathbf{r}}$) to a rotation of π. In general, we have $K_l \neq K_t$.

In addition, to quartic order there will appear a term contributing to $S_{\rm C}$ of the form

$$S^{AT}_{\rm C} = -K_4 \; \beta \sum_{\langle \mathbf{r},\mathbf{r}'\rangle} J^x_{\mathbf{r}} J^x_{\mathbf{r}'} J^y_{\mathbf{r}} J^y_{\mathbf{r}'}, \quad (2)$$

which is seen to represent a coupling term of the form appearing in the well-known Ashkin–Teller (AT) model[15], for which several exact results are known[16]. There will also be other terms appearing to quartic order, most of which either are constants or renormalize the quadratic piece of the action. Note that four Ising variables of two distinct species all located on one single lattice site simply contributes a constant to the action. If we now limit ourselves to terms that have four J-fields distributed on two nearest neighbor lattice sites, there only two distinct possibilities. Firstly, we may have a term with three J's on one lattice site and one J on a nearest-neighbor site. This merely represents a renormalization of the quadratic couplings. Secondly, we may have two J's on one lattice site and another two on a nearest neighbor. Unless there are two distinct species of J's on each of the lattice sites, such a term will represent a constant contribution to the action. If the J's on each lattice site are of distinct species, the term will be of the AT-form, as written above. We will ignore terms that have J-fields distributed on three or four distinct lattice sites, as these are generated by much higher order terms in t_{pd}, t_{pp}.

Note that although the K_x and K_y couplings between the two different types of Ising fields in this model are anisotropic[3,4,17], there is only one (doubly degenerate) Ising transition in the system for $K^{xy} = 0; K_4 = 0$. Hence, when we introduce the AT coupling, the Ising critical point evolves into a single phase-transition line with non-universal critical exponents. In particular, the specific heat exponent α becomes negative, with the transition line itself being a selfdual critical line[16]. In this sense, the model is similar to an *isotropic* AT model, where the exact result for the critical exponents are known, and for instance given by[16] $\alpha = (2-2y)/(3-2y)$ and $\beta = (2-y)/(24-16y)$. From this, we deduce the susceptibility exponent $\gamma = (14-7y)/(12-8y)$ and the correlation length exponent $\nu = (2-y)/(3-2y)$. Here $y = 2\mu/\pi$ and $\cos(\mu) = [e^{4K_4}-1]/2$. Hence, for $K_4 \leq 0$, we have $\pi/2 \leq \mu < 2\pi/3$, such that $1 \leq y < 4/3$. These exponents are plotted in Fig. 2. The most extreme deviation from the $2D$ Ising values $\alpha = 0, \beta = 1/8, \gamma = 7/4, \nu = 1$ is given by the case $K_4 \to -\infty, y = 4/3$, where $\alpha = -2, \beta = 1/4, \gamma = 7/2, \nu = 2$. Note the weak variation in β as a function of K_4. It is the evolution of the anomaly in the specific heat, concomitant with the evolution of the staggered orbital magnetic moment as well as the susceptibility of the staggered orbital magnetic moment as we vary K_4 in $\mathcal{S}_{\rm C} = S_{\rm C} + S^{AT}_{\rm C}$ in Eqs. 1 and 2, which will be considered in this paper. The specific heat C_v is given by

$$C_v = \frac{1}{L^2} \langle (\mathcal{S}_{\rm C} - \langle \mathcal{S}_{\rm C}\rangle)^2 \rangle. \quad (3)$$

We will also consider the staggered order parameter and its susceptibility. Considering Fig. 3, we see that we may define a pseudo-"spin" $\mathbf{S}$ on each lattice given by $\mathbf{S}_{\mathbf{r}} \equiv (J^x_{\mathbf{r}}, J^y_{\mathbf{r}})$. The various states of the system are then described by a 4-state clock pseudospin $\mathbf{S}_{\mathbf{r}} = (\pm 1, \pm 1)$ on a 2-dimensional square lattice. We define the staggered order parameter in the standard way it would be defined for a clock model, namely

$$M_{\rm so} \equiv \sqrt{\frac{\langle m^x\rangle^2 + \langle m^y\rangle^2}{2}}, \quad (4)$$

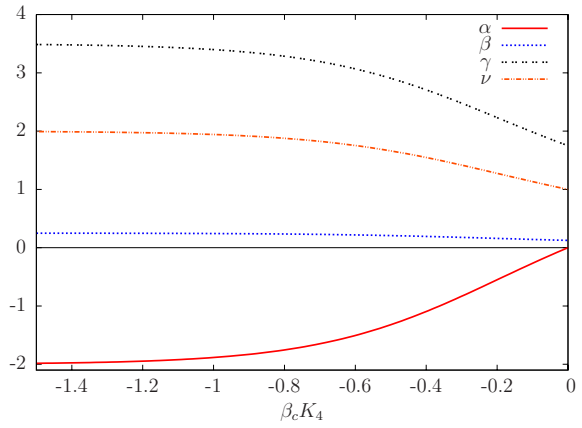

FIG. 2: (Color online) Critical exponents α, β, and γ from the Ashkin–Teller model, as a function of the four-spin coupling $\beta_c K_4 \leq 0$[16]. In this parameter range, we have $-2 < \alpha \leq 0$, $1/8 \leq \beta < 1/4$, and $7/4 \leq \gamma < 7/2$, $1 \leq \nu < 2$.

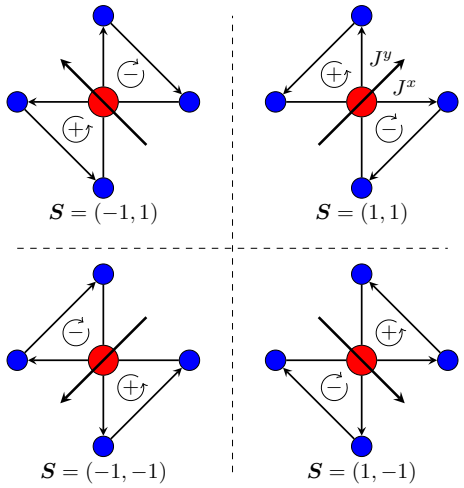

FIG. 3: (Color online) An illustration of the pseudo-"spin" $\mathbf{S} = (J^x_{\mathbf{r}}, J^y_{\mathbf{r}})$ we use to compute the staggered order parameter and its susceptibility, Eqs. 4 and 5.

where $m^\alpha \equiv \sum_{\mathbf{r}} J^\alpha_{\mathbf{r}}, \alpha \in (x, y)$. Furthermore, we will consider the susceptibility of this staggered order parameter, given by

$$\chi_{\rm M} = \frac{1}{L^2} \sum_{\alpha=x,y} \left[\langle (m^\alpha)^2 \rangle - \langle m^\alpha \rangle^2 \right]. \tag{5}$$

We will contrast these quantities with the evolution of the anomaly in the specific heat as the parameter K_4 is varied. While the above staggered moment does not couple linearly to an external uniform magnetic field, it will couple to a field-induced uniform magnetic moment via a quartic term in the free energy. The field-induced uniform magnetisation will therefore have a non-analytic behavior across the phase transition where the staggered magnetisation associated with the ordering of the orbital currents sets in. We will return to this point at the end of Section II.

For the purposes of extracting critical exponents, we will consider the Binder cumulant, defined by

$$G \equiv \frac{\langle m^4 \rangle}{\langle m^2 \rangle^2}, \tag{6}$$

where $m^2 = (m^x)^2 + (m^y)^2$. In the ordered phase, $G = 1$. For an N-component order parameter, $G = (N + 2)/N$ in the disordered phase. In our case, therefore, G will exhibit a rise from 1 to 2 as the systems disorders. When computing this quantity for different L and plotting it as a function of T, the curves will cross at the same point, thus defining T_c. On the other hand, plotting it as a function of $L^{1/\nu}|(T - T_c)/T_c)|$, all the curves will collapse on each other. By adjusting ν to get data-collapse, one obtains the correlation length exponent. Furthermore, the order-parameter exponent β is obtained from the magnetisation M_{so} for various system sizes by considering the quantity $L^{\beta/\nu} M_{so}$ and adjusting β and ν so as to obtain data-collapse when plotting this quantity as a function of $L^{1/\nu}|(T - T_c)/T_c)|$.

II. MONTE-CARLO RESULTS

The Monte-Carlo computations were performed using the standard single-spin update Metropolis-Hastings algorithm[18,19], making local updates of the Ising-fields $J^x_{\mathbf{r}}$ and $J^y_{\mathbf{r}}$, as well as local updates of the composite Ising-field $J^x_{\mathbf{r}} J^y_{\mathbf{r}}$ at each lattice site. The system-grid is defined by two 2-dimensional subgrids, one for each Ising-field, and the local updates were performed for all points on the grid. All the Ising-fields on both subgrids were initially set to 1. We started all simulations at the high-temperature end, and discarded the first 100000 sweeps for the purposes of initial thermalization. After that, measurements were made for every 100 sweeps. For each value of β, we ran up to $3 \cdot 10^6$ MC sweeps, and after each sweep the total energy as well as the staggered magnetisation within each unit cell $M_{\rm so}$ on each subgrid, were saved to file. During the computations, we sampled the specific heat C_v and the susceptibility $\chi_{\rm M}$. The system sizes that were considered were $L \times L$ with $L = 32, 64, 128, 256$. In all simulations, we have set $K_l = 1.0$, such that all other couplings are measured relative to this parameter. In these units, the inverse critical temperature β_c of the system for $A = 1.0, K_3 = 0, K_4 = 0$ is given by $\beta_c = \ln(1 + \sqrt{2})/2 \approx 0.44$. This sets the scale of the critical couplings in the plots we will show below.

A. Specific heat

Let us first investigate what effect K_3 has on the logarithmic singularity of the $2D$ Ising model. In Fig. 4, we show the specific heat anomaly for $A = 1.0$ and $K_4 = 0$, upon varying $K_3 = 0.0, 0.1, 0.2, 0.3$. We limit the variations in K_3 so as to remain within a state of uniformly

ordered current-patterns and to avoid orbital current patterns exhibiting striped order. It is seen that the K_3 term leaves the logarithmic singularity of the anisotropic double-Ising-model (Eq. 1 with $K_3 = 0, K_4 = 0$) unaltered, only the amplitude of the anomaly is changed. This is easily understood, since we may write the classical part of the model for general A and finite K_3 on the form[3,4]

$$S_{\rm C} = -\beta \left\{ \sum_{\langle \mathbf{r},\mathbf{r}' \rangle} \left[\bar{K} \, \cos(\theta_{\mathbf{r}} - \theta_{\mathbf{r}'}) + \Delta K \, \sin(\theta_{\mathbf{r}} + \theta_{\mathbf{r}'}) \right] + 2 \sum_{\langle\langle \mathbf{r},\mathbf{r}' \rangle\rangle} K^{xy} \, \cos(\theta_{\mathbf{r}} + \theta_{\mathbf{r}'}) \right\}, \tag{7}$$

where we have defined $\bar{K} = K_x + K_y$, $\Delta K = K_x - K_y$, and we have parametrised the action in terms of the angles $\theta_{\mathbf{r}'\tau}$ defined by $\cos(\theta_{\mathbf{r}'\tau}) = [J^x_{\mathbf{r}}(\tau) + J^y_{\mathbf{r}}(\tau)]/2$ and $\sin(\theta_{\mathbf{r}'\tau}) = [J^x_{\mathbf{r}}(\tau) - J^y_{\mathbf{r}}(\tau)]/2$. The Ising character of the fields $J^x_{\mathbf{r}}(\tau)$ and $J^y_{\mathbf{r}}(\tau)$ then implies that $\theta_{\mathbf{r}\tau} \in (0, \pi/2, \pi, 3\pi/2)$. The latter restriction on $\theta_{\mathbf{r}}$ implies that $\theta_{\mathbf{r},\tau} - \theta_{\mathbf{r}',\tau}$ and $\theta_{\mathbf{r},\tau} + \theta_{\mathbf{r}',\tau}$ differ by an integer multiple of π. Therefore, under a global Z_4 symmetry operation on the fields $\theta_{\mathbf{r}} \to \theta'_{\mathbf{r}} = \theta_{\mathbf{r}} + n\pi/2; n = 1, 2, 3$, the transformed quantities $\theta'_{\mathbf{r},\tau} - \theta'_{\mathbf{r}',\tau}$ and $\theta'_{\mathbf{r},\tau} + \theta'_{\mathbf{r}',\tau}$ will differ globally by an integer multiple of π, which at most leads to a global sign-change in the last two terms in Eq. 7. However, by the definitions given for K_x, K_y and K^{xy} below Eq. 2, it is clear that the sign of these coefficients is immaterial since a sign change may be compensated by interchanging K_l and K_t and changing the sign of K_3. The model is therefore a global Z_4-symmetric model, which is equivalent to the original $Z_2 \times Z_2$-symmetry. Hence, introduction of K_3 does not alter the Ising symmetry of the problem, and therefore the universality class of the phase-transition is unaltered (as long as we consider a phase-transition for a uniformly ordered to a completely disordered state).

We now investigate the effect of including K_4. Note that in terms of the variable $\theta_{\mathbf{r}}$, the AT-term in Eq. 2 may be written on the form (again replacing $\int_0^\beta d\tau$ with β and omitting the τ-dependence of the fields)

$$\begin{aligned} S^{AT}_{\rm C} &= -\beta \, K_4 \sum_{\langle \mathbf{r},\mathbf{r}' \rangle} \cos(2\theta_{\mathbf{r}}) \cos(2\theta_{\mathbf{r}'}) \\ &= -\beta \, K_4 \sum_{\langle \mathbf{r},\mathbf{r}' \rangle} \cos(2(\theta_{\mathbf{r}} - \theta_{\mathbf{r}'})) \, . \end{aligned} \tag{8}$$

In the last equality, we have used the fact that $2(\theta_{\mathbf{r}} - \theta_{\mathbf{r}'})$ differs from $2(\theta_{\mathbf{r}} + \theta_{\mathbf{r}'})$ by an integer multiple of 2π with our restrictions on $\theta_{\mathbf{r}}$. Eq. 8 exhibits a local Ising-symmetry in addition to the global Ising symmetry. Namely, one can make *local* changes $J^x_{\mathbf{r}}(\tau) \to -J^x_{\mathbf{r}}(\tau)$ and $J^y_{\mathbf{r}}(\tau) \to -J^y_{\mathbf{r}}(\tau)$, equivalently local changes in $\theta_{\mathbf{r}}$ in multiples of π. These are symmetries that the previously discussed terms do not have. Hence, $S^{AT}_{\rm C}$ changes the global $Z_2 \times Z_2$-symmetry of the problem, and we thus expect changes in the specific heat anomalies when K_4 is introduced. We emphasize that we will only consider negative K_4 in this paper. A positive K_4 will lead to stronger specific heat singularities than in the $2D$ Ising case. It is therefore clear *a priori* that the effective theory of Eqs. 1 and 2 with $K_4 > 0$ is not a viable theory for the pseudogap-line.

We first consider the case of isotropic Ising coupling $K_l = K_t$, i.e. $A = 1.0$, next-nearest neighbor coupling $K_3 = 0.0$, and increasing $|K_4|$. We use this case for reference, as this parameter set represents the standard isotropic AT model[15,20]. The results for the specific heat are shown in Fig. 5. A substantial suppression of the logarithmic specific heat-anomaly of the Ising model is clearly seen, as $|K_4|$ increases.

We next consider the effect of increasing the anisotropy ($A < 1$), such as to weaken the ordering in each of the $J_y(\mathbf{r})$- and $J_x(\mathbf{r})$ Ising fields. Note, however, that because the anisotropy introduced is equal for both of the Ising fields (only the direction of the anisotropy is changed) the model only has one single critical point even in the absence of a K_4-coupling. The model is then merely two copies of one and the same anisotropic $2D$ Ising model. However, an increase in $|K_4|$ is expected to have a stronger effect for $A < 1.0$ than when $A = 1.0$, due to weaker ordering and lower critical temperature when $A < 1.0$. This enhancement of the anomaly-suppression is indeed seen in Fig. 6 compared to Fig. 5.

We will now repeat the above computations for $A = 1.0$ with $K_3 = 0.1, 0.2$ and 0.3. This coupling will tend to frustrate the Ising ordering, since the presence of K_3 tends to promote striped order instead of uniform ordering in the Ising-fields, due to the diagonal anisotropy (represented by a change of sign in K_3 upon $\pi/2$ rotations of next-nearest neighbor vectors). It is of interest to see how the presence of K_3 affects the introduction of the AT coupling K_4. Naively, since the coupling K_3 promotes striped order and frustrates the uniform order promoted by K_x, K_y, we would in principle expect that the suppressed anomalies are pushed to lower temperatures when K_3 is increased. In Figs. 7, 8, and 9, we show the specific heat anomaly for the same sets of parameters as in Fig. 5, except that now $K_3 = 0.1, 0.2, 0.3$, respectively.

Again, we see a substantial suppression of the specific heat anomaly, although the suppressed features appear

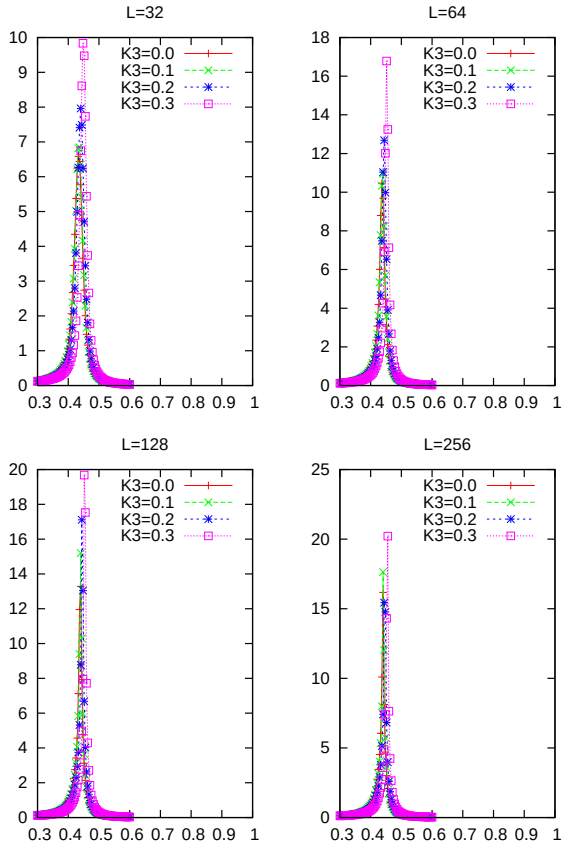

FIG. 4: (Color online) Specific heat anomaly as a function of inverse temperature $1/T$ for the classical part of the model in Eqs. (1) and (2), with $A = 1.0$ and $K_4 = 0.0$, for various values of $K_3 = 0.0, 0.1, 0.2, 0.3$, and various system sizes $L = 32, 64, 128, 256$. The amplitude of the logarithmic specific heat of the Ising model ($K_3 = 0$), is enhanced as K_3 increases, but the anomaly remains logarithmic. The K_3-term does not alter the global $Z_2 \times Z_2$-symmetry of the anisotropic double-Ising-model. Note also that for this set of parameters, K_3 hardly alters the critical coupling $\beta_c \approx 0.44$ of the model with $K_3 = 0$.

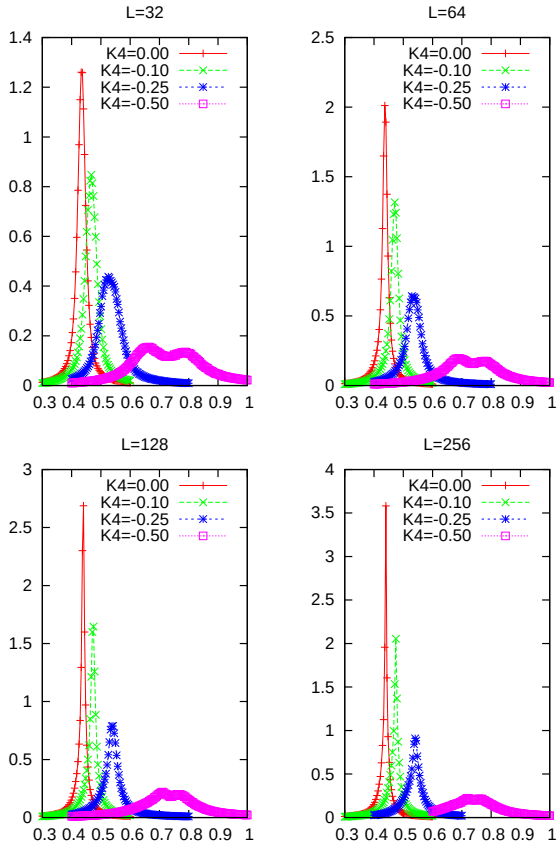

FIG. 5: (Color online) Specific heat anomaly as a function of inverse temperature $1/T$ for the classical part of the generalized AT model Eqs. (1) and (2), with $A = 1.0$ and $K_3 = 0.0$, for various values of $K_4 = 0.0, -0.1, -0.25, -0.3, -0.5$, and various system sizes $L = 32, 64, 128, 256$. The logarithmic specific heat of the Ising model ($K_4 = 0$), is seen to be strongly suppressed as $|K_4|$ increases.

to become sharper. We also see that the anomalies that remain are pushed slightly downwards in temperature compared to the case $K_3 = 0$, cf. the lower right panel in Fig. 5. The change is however only minor for the cases $K_3 = 0.1$ and $K_3 = 0.2$, consistent with the weak suppression of the critical temperature we found upon increasing K_3 in Fig. 4. However, for $K_3 = 0.3$ this is no longer the case. The conclusion we draw from these computations is that it is indeed possible to obtain a drastic reduction of the specific heat anomaly compared to the Ising case when an Ashkin-Teller coupling K_4 is included, but that the parameter K_3 impedes the reduction of the anomaly.

Finally, we consider the most general case of anisotropic Ising coupling $A = 0.5$ and finite $K_3 = 0.3$, as $|K_4|$ is increased, shown in Fig. 10. It is clear from Fig. 10 that the introduction of anisotropy $A = K_t/K_l = 0.5$ appears to facilitate the reduction of the specific heat anomaly. This is easily understood, since increasing anisotropy implies that the magnitude of K_4 relative to the Ising couplings in the problem will increase. The effect of a given increase in K_4 will therefore be more strongly felt. Moreover, as in the isotropic case, the anomalies are pushed down in temperature compared to the case $K_3 = 0$, cf. the lower right panel of Fig. 6.

B. Order parameter and susceptibility

Let us now study the order parameter and susceptibility of the order parameter, $M_{\rm so}$ and $\chi_{\rm M}$, Eqs. 4 and 5. We have chosen parameters $A = 1.0$, $K_3 = 0$, and varied K_4, for which the evolution of the specific heat anomaly is shown in Fig. 5. The results for M_{so} and $\chi_{\rm M}$ are shown in Figs. 11 and 12, respectively. We see that the staggered magnetisation retains a non-analytic behavior as in the pure Ising case even for $K_4 = -0.5$. This contrasts

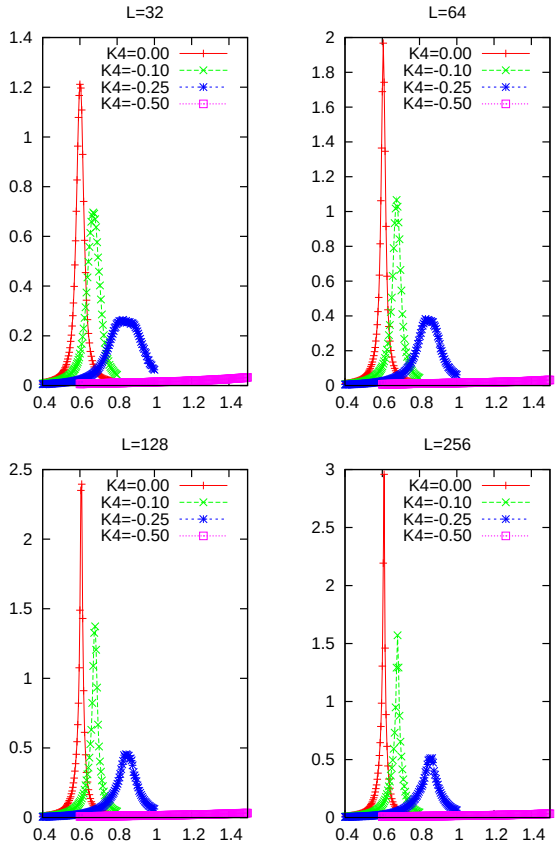

FIG. 6: (Color online) Specific heat anomaly as a function of inverse temperature $1/T$ for the classical part of the generalized AT model Eqs. (1) and (2), with $A = 0.5$ and $K_3 = 0.0$, for various values of $K_4 = 0.0, -0.1, -0.25, -0.3, -0.5$, and various system sizes $L = 32, 64, 128, 256$. Compared to the case shown in Fig. 5, with $A = 1.0$, precisely the same trends are seen in the evolution of the anomaly as the AT coupling $|K_4|$ is increased, only slightly more pronounced.

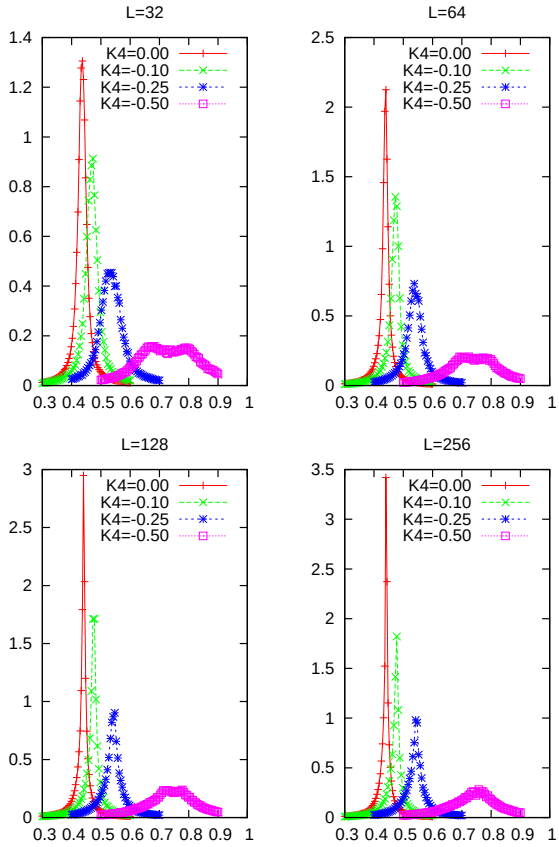

FIG. 7: (Color online) Specific heat anomaly as a function of inverse temperature $1/T$ for the classical part of the generalized AT model Eqs. (1) and (2), with $A = 1.0$ and $K_3 = 0.1$, for various values of $K_4 = 0.0, -0.1, -0.25, -0.3, -0.5$, and various system sizes $L = 32, 64, 128, 256$.

sharply with the lack of any traces of singular behavior in the specific heat, cf. Fig. 5. From Fig. 12 we see the same trend, namely that the susceptibility retains a non-analytic feature even for the largest K_4 values we have considered, and which suffice to completely suppress the anomalies in the specific heat. Moreover, by inspecting these results in more detail, we see from Fig. 12 that the peak-height in $\chi_{\rm M}$ evolves quite differently as a function of system size L for the cases $K_4 = 0$ and $K_4 = -0.5$. The peak height in $\chi_{\rm M}$ has a much more rapid growth for the latter case. This indicates that the susceptibility exponent γ increases when $-K_4$ increases. This is consistent with known results for Ashkin–Teller exponents[16]. We have not attempted a detailed finite-size scaling analysis to actually determine the precise values of the critical exponents for our model. We have repeated these calculation also with $K_3 = 0.3$. The results are shown in Figs. 13 and 14, with essentially the same results as in Figs. 11 and 12.

The above has interesting ramifications for thermodynamic signals across the phase transition for the system in a uniform external magnetic field. Such a magnetic field will induce a uniform magnetisation in the system that couples to the staggered magnetisation. Hence, an onset of the staggered magnetisation at the phase transition will induce a *non-analytic reduction* of the *uniform* field-induced magnetisation across the phase transition.

To investigate this point in detail, we consider a simple Ginzburg–Landau theory of a system exhibiting staggered magnetisation M_{so} in a uniform external magnetic field H. Such an external field will induce a uniform magnetisation M_0 in the system, but does not couple directly to the staggered magnetisation M_{so}, and hence H will not destroy the phase transition in the M_{so} sector. We assume for simplicity that the magnetic moments are of Ising character, consistent with what we have done so far. Hence, the Ginzburg–Landau free energy of the system at the mean-field level is given by

$$\begin{aligned} F &= \frac{a_s}{2}M_{so}^2 + \frac{a_0}{2}M_0^2 - HM_0 \\ &+ \frac{u_s}{4}M_{so}^4 + \frac{u_0}{4}M_0^4 + \frac{u_{0s}}{2}M_{so}^2M_0^2. \end{aligned} \tag{9}$$

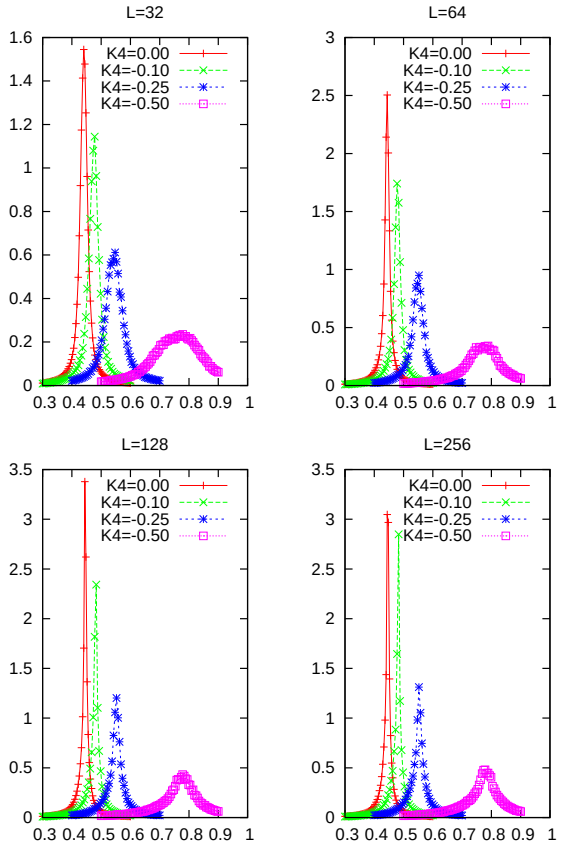

FIG. 8: (Color online) Specific heat anomaly as a function of inverse temperature $1/T$ for the classical part of the generalized AT model Eqs. (1) and (2), with $A = 1.0$ and $K_3 = 0.2$, for various values of $K_4 = 0.0, -0.1, -0.25, -0.3, -0.5$, and various system sizes $L = 32, 64, 128, 256$.

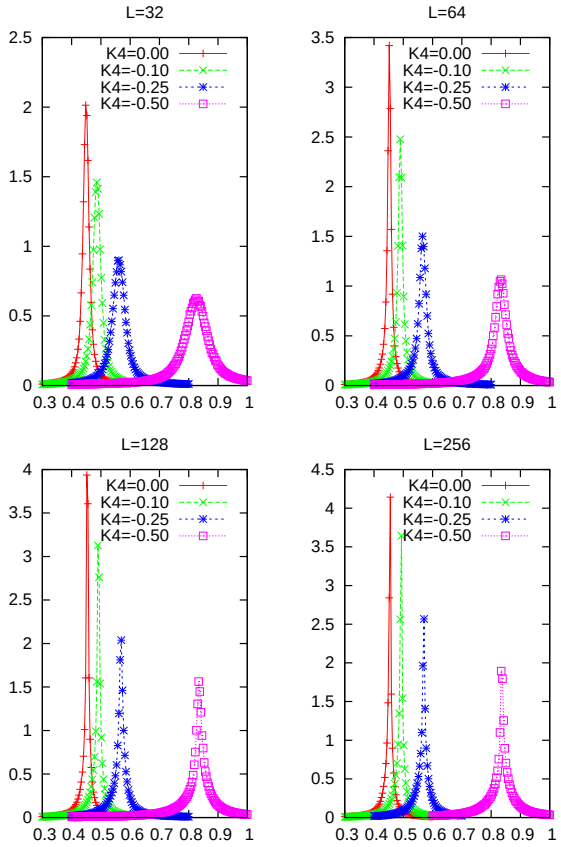

FIG. 9: (Color online) Specific heat anomaly as a function of inverse temperature $1/T$ for the classical part of the generalized AT model Eqs. (1) and (2), with $A = 1.0$ and $K_3 = 0.3$, for various values of $K_4 = 0.0, -0.1, -0.25, -0.3, -0.5$, and various system sizes $L = 32, 64, 128, 256$.

Here, a_s changes sign when the temperature passes through the zero-field critical temperature of the system, where staggered orbital magnetic ordering sets in. We have that $a_s > 0, T > T_c$, and $a_s < 0, T < T_c$. Close to T_c, we have $a_s(T) = a_s^0(T - T_c)$. Moreover, $a_0 > 0$ for all T, since we will assume that the uniform magnetisation is zero in the absence of an external magnetic field H, and on quite general grounds we may assume that $(u_s, u_0, u_{0s}) > 0$. Now, minimising this free energy with respect to M_{so} and M_0 and solving for the uniform magnetisation, we obtain

$$M_0 = \frac{H}{a_0 + u_{0s} M_{so}^2}. \tag{10}$$

Furthermore, we have

$$M_{so} = \begin{cases} 0 & T > T_c \\ C|T - T_c|^\beta & T < T_c, \end{cases} \tag{11}$$

where the second equality holds when $|T - T_c|/T_c \ll 1$. Since Eq. 11 represents a non-analytic temperature dependence, Eq. 10 will also feature a non-analyticity as a function of temperature. This result is completely generic to any system which features a zero-field staggered order parameter, when a uniform external magnetic field is introduced. At the mean-field level, we have $\beta = 1/2$. Including fluctuations, which are severe in $2D$, gives a result for M_{so} of identical form with a fluctuation renormalized β which will be close to the non-universal value obtained from the Ashkin–Teller model[16]. Hence, we predict that a measurement of the uniform magnetisation of the system across the pseudogap line will result in a *non-analytic reduction of the uniform magnetisation as one crosses the pseudogap line from high to low temperatures* given by the expression

$$\frac{H}{M_0} = A + B\ \Theta(T_c - T)\ \left|1 - \frac{T}{T_c}\right|^{2\beta}. \tag{12}$$

Here, β is the *staggered* order-parameter exponent which should be non-universal, $\Theta(x)$ is the Heaviside step function $\Theta(x) = 0, x < 0; \Theta(x) = 1, x > 0$. Moreover, A and B are essentially temperature-independent inverse uniform and staggered magnetic susceptibilities, respectively. Non-universality in β due to the presence of the

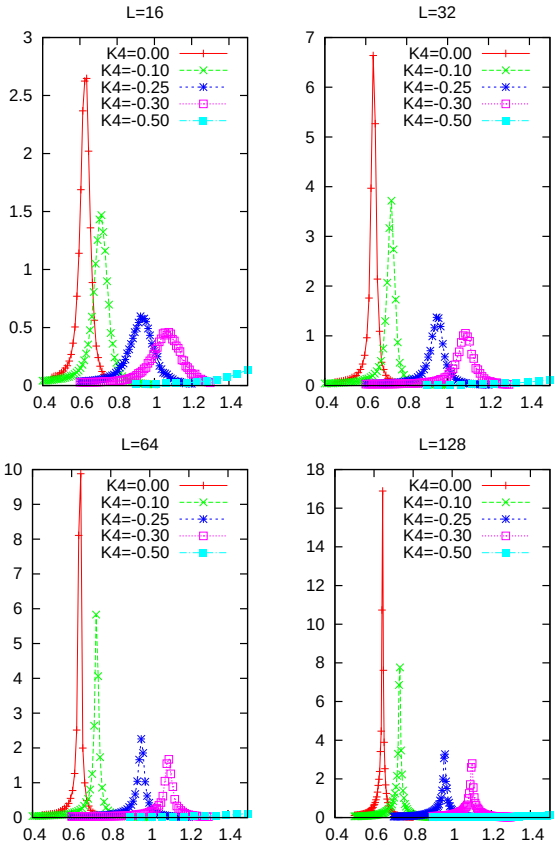

FIG. 10: (Color online) Specific heat anomaly as a function of inverse temperature $1/T$ for the classical part of the generalized AT model Eqs. (1) and (2), with $A = 0.5$ and $K_3 = 0.3$, for various values of $K_4 = 0.0, -0.1, -0.25, -0.3, -0.5$, and various system sizes $L = 32, 64, 128, 256$.

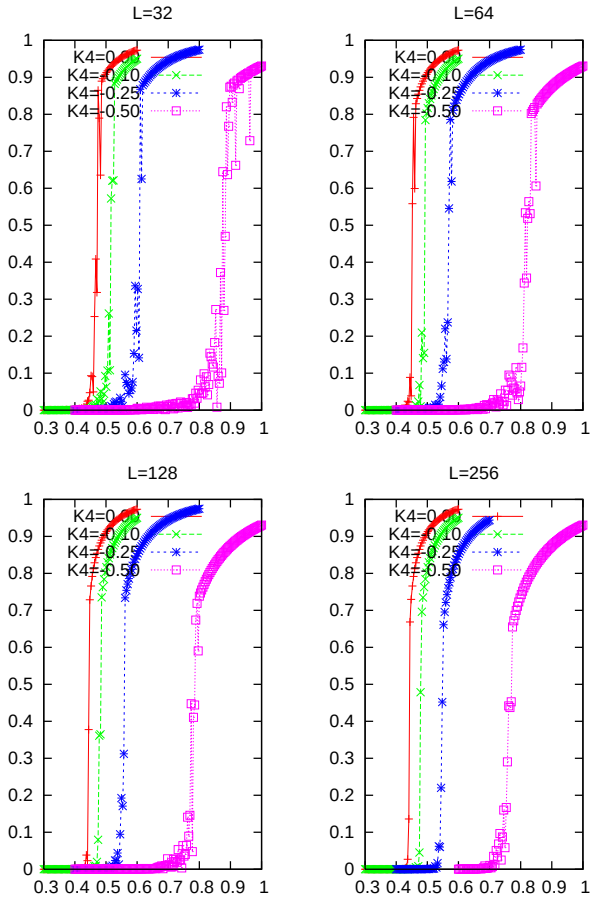

FIG. 11: (Color online) The staggered order parameter, Eq. 4, as a function of inverse temperature $1/T$ for the classical part of the generalized AT model Eqs. 1 and 2, with $A = 1.0$ and $K_3 = 0.0$, for various values of $K_4 = 0.0, -0.25, -0.5$, and various system sizes $L = 32, 64, 128, 256$.

parameter K_4 in the problem means that β in principle should vary slightly as we cross the pseudogap line vertically in the (x, T)-phase diagram of high-T_c cuprates as the doping is varied. This is clearly seen from Fig. 11. We also note from Fig. 4 that introduction of K_3 does not change the universality class of the transition when $K_4 = 0$. We may therefore quite reasonably assume that the presence of K_3, which does not change the Ising symmetry of the problem, does not change the Ashkin–Teller universality class of the phase transition when K_4 is present. We may then deduce that for negative K_4, we will have $-2 < \alpha < 0$, $1/8 < \beta < 1/4$, and $7/4 < \gamma < 7/2$. A strong suppression of the specific heat anomaly as seen for the case $K_4 = -0.5$, puts us at $\alpha \approx -1.3$, $\beta \approx 0.2$, and $\gamma \approx 2.9$[23]. The weak variation in the exponent β from the Ising value $1/8$ is due to the near-cancellation of the rather large, but opposite, variations in the specific-heat exponent α and the susceptibility-exponent exponent γ, consistent with the scaling law $\alpha + 2\beta + \gamma = 2$. It is precisely the large variation in α that wipes out the specific-heat anomaly that also produces a large enhancement of the susceptibility of the staggered orbital magnetisation.

III. SUMMARY

In summary, we have studied the evolution of a specific heat anomaly in an effective theory of fluctuating orbital currents in high-T_c cuprates. The motivation for the work has been to see if the finite-temperature break-up of a proposed Ising-ordering associated with an ordered circulating current pattern would be a viable mechanism for explaining the pseudogap-line of high-T_c cuprates on the underdoped side. This is a first step towards investigating whether or not the quantum break-up of such order could give rise to quantum critical fluctuations that could possibly explain the anomalous transport properties in the normal state of these compounds. A necessary requirement is then that the proposed Ising-ordering is destroyed at finite temperature in the underdoped side via a second order phase-transition which does not exhibit an

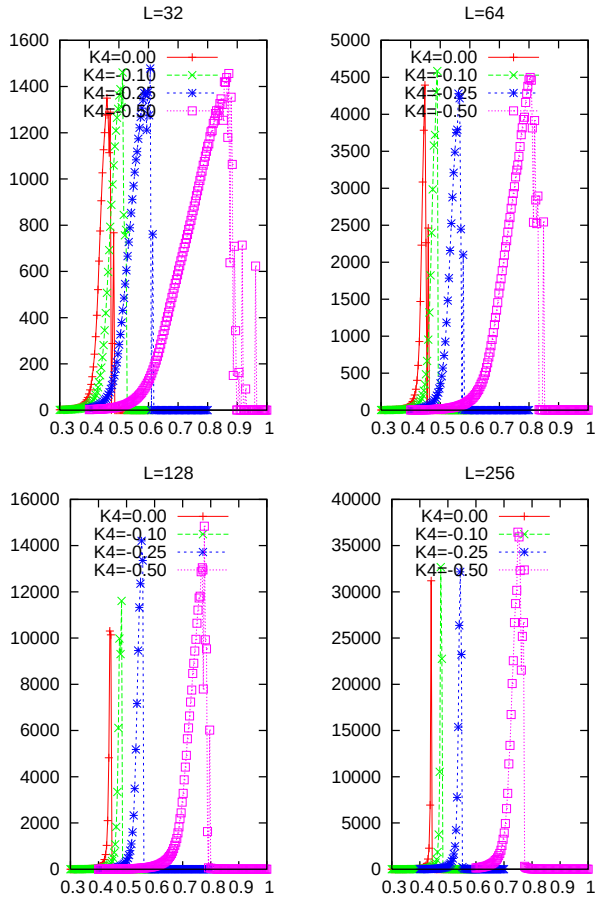

FIG. 12: (Color online) The susceptibility of the staggered magnetisation within each unit cell, Eq. 5 , as a function of inverse temperature $1/T$ for the classical part of the generalized AT model Eqs. 1 and 2, with $A = 1.0$ and $K_3 = 0.0$, for various values of $K_4 = 0.0, -0.25, -0.5$, and various system sizes $L = 32, 64, 128, 256$. Note that the susceptibility retains the non-analytical features of the Ising-case even for parameters where the specific heat anomaly is completely suppressed.

easily detectable logarithmic singularity. In this paper, we have shown that the effective field theory of a particular proposed hidden order in the form of long-range correlation between orbital currents within a CuO_2-plane passes this test by destroying the Ising-order while exhibiting no singularity in the specific heat, only weak anomalies that do not scale with system size. Moreover, we predict that a field-induced uniform magnetisation will feature a non-analytic behavior as a function of temperature as the phase transition is crossed. This is a consequence of the non-analytic behavior of the staggered magnetisation across the transition, which couples to the uniform magnetisation via a fourth order term.

Acknowledgments. This work was supported by the Norwegian Research Council Grants No. 158518/431 and No. 158547/431 (NANOMAT), and Grant No. 167498/V30 (STORFORSK). The authors acknowledge communications and discussions with M. Greiter, J. Linder, M. Wallin, and Z. Tesanovic.

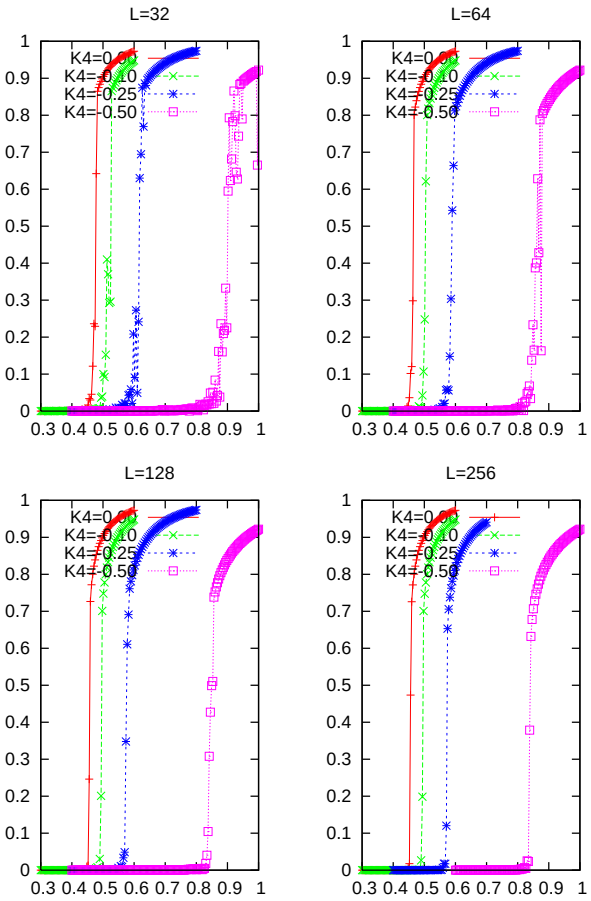

FIG. 13: (Color online) The staggered order parameter, Eq. 4, as a function of inverse temperature $1/T$ for the classical part of the generalized AT model Eqs. 1 and 2, with $A = 1.0$ and $K_3 = 0.3$, for various values of $K_4 = 0.0, -0.25, -0.5$, and various system sizes $L = 32, 64, 128, 256$.

[1] C. M. Varma, Phys. Rev. B **73**, 155113 (2006).
[2] C. M. Varma, P. B. Littlewood, S. Schmitt-Rink, E. Abrahams, and A. E. Ruckenstein, Phys. Rev. Lett, **63**, 1996 (1989).
[3] K. Børkje and A. Sudbø, Phys. Rev. B **77**, 092404 (2008); `arXiv:0801.4611`.
[4] K. Børkje, *Theoretical Studies of Unconventional Order in Quantum Many-Particle Systems*, PhD Thesis, Norwegian University of Science and Technology, (2008).
[5] A. Sudbø, S. Schmitt-Rink, and C. M. Varma, Phys. Rev. B **46**, 5548 (1992).
[6] A. Sudbø, C. M. Varma, T. Giamarchi, E. B. Stechel, and

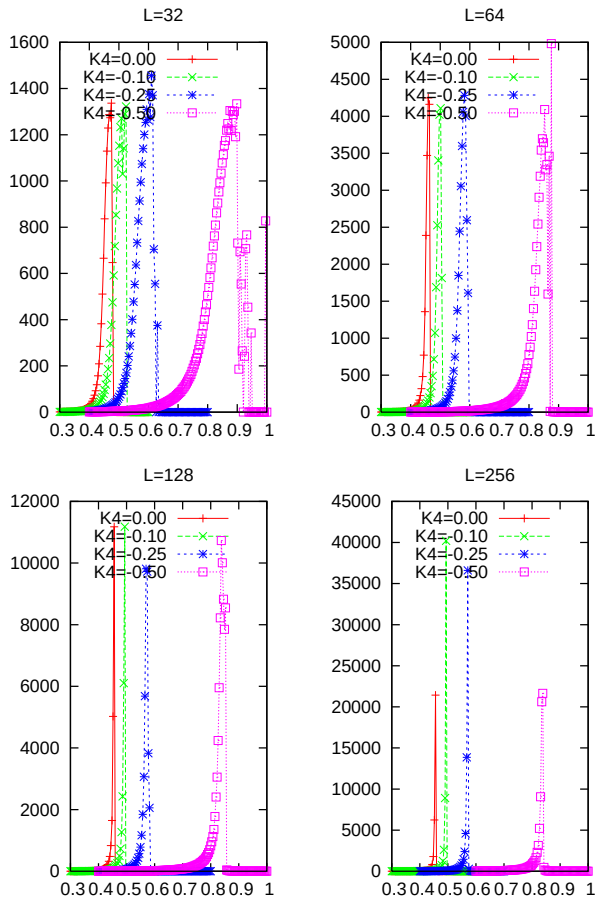

FIG. 14: (Color online) The susceptibility of the staggered magnetisation within each unit cell, Eq. 5 , as a function of inverse temperature $1/T$ for the classical part of the generalized AT model Eqs. 1 and 2, with $A = 1.0$ and $K_3 = 0.3$, for various values of $K_4 = 0.0, -0.25, -0.5$, and various system sizes $L = 32, 64, 128, 256$.

R. T. Scalettar, Phys. Rev. Lett. **72**, 3292 (1994).

[7] A. W. Sandvik and A. Sudbø, Phys. Rev. B **54**, R3746 (1996).

[8] C. M. Varma, Phys. Rev. B **55**, 14554 (1997).

[9] H. C. Lee and H.-Y. Choi, Phys. Rev. B bf 64, 094508 (2001).

[10] S. Chakravarty, R. B. Laughlin, D. K. Morr, and C. Nayak, Phys. Rev. B **63**, 094503 (2001).

[11] B. Fauqué, Y. Sidis, V. Hinkov, S. Pailhes, C. T. Lin, X. Chaud, and P. Bourges, Phys. Rev. Lett., **96**, 197001 (2006).

[12] H. A. Mook, Y. Sidis, B. Fauqué, V. Balédent, and P. Bourges, `arXiv:0802.3620`.

[13] The orbital-current fluctuations that are driven by V in this model have an interesting counterpart in one dimension, where several essentially exact results are known, see Refs.[5–7]. In these works, a repulsive V drives $Cu - 0$ charge fluctuations that promote charge-transfer instabilities or superconductivity in these $Cu-O$-chains away from half-filling for parameters that give an antiferromagnetic Mott-Hubbard insulator at half filling. However, these charge fluctuations are completely suppressed if all doubly-occupied sites are projected out of the Hilbert space. It is therefore quite possible that the orbital current patterns driven by V depicted in Fig. 1 may also be suppressed by a similar truncation of the Hilbert space for the CuO_2-sheets.

[14] A recent numerical evaluation of the current-current correlations in a three-band $t - J$-model with 24 sites, where doubly occupied sites have been projected out, shows no evidence of the orbital current pattern in Fig. 1, see M. Greiter and R. Thomale, Phys. Rev. Lett., **99**, 027005 (2007). While the results may be accurate for the model that is actually studied, it is not obviously an accurate representation of the full three-band CuO_2-model. However, a variational Monte Carlo study of the full three-band model on a much larger system with 8×8 unit cells does show evidence for the orbital current ordering in Fig. 1, T. Giamarchi, Talk at the APS March Meeting, New Orleans, 2008.

[15] J. Ashkin and E. Teller, Phys. Rev. **64**, 178 (1943).

[16] R. J. Baxter, *Exactly Solved Models in Statistical Mechanics*, Academic Press (London), (1982).

[17] Anisotropy is generic to bond-variables, which, unlike site-variables, have *directionality*. In the present paper we treat a problem in the particle-hole channel. See however also A. Melikyan and Z. Tesanovic, Phys. Rev. B **71**, 214511 (2005), and Z. Tesanovic, `arXiv:0705.3836`. These authors treat a problem in the particle-particle channel, namely the case of a phase-fluctuating lattice d-wave superconductor where the phase is a bond-variable.

[18] N. Metropolis, A. W. Rosenbluth, M. N. Rosenbluth, A. H. Teller, and E. Teller, J. Chem. Phys., **21**, 1087 (1953).

[19] W. K. Hastings, Biometrika, **57**, 97 (1970).

[20] V. Aji and C. M. Varma, Phys. Rev. Lett., **99**, 067003 (2007).

[21] J. V. José, L. P. Kadanoff, S. Kirkpatrick, and D. R. Nelson, Phys. Rev. B **16**, 1217 (1977).

[22] L. P. Kadanoff and A. C. Brown, Ann. og Phys., **121**, 318 (1979).

[23] In spin-polarised neutron scattering experiments, Ref. 12 reports a non-analytic change in the scattering intensity at the pseudogap temperature (T_c in our notation) of the form $I = I_0 + I_1|1 - T/T_c|^{2\beta}$, with a $2\beta = 0.37 \pm 0.12$. This is within the rather narrow upper and lower bound on β imposed by the generalised Ashkin–Teller model Eqs. 1 and 2.